The author(s) shown below used Federal funds provided by the U.S. Department of Justice and prepared the following final report:

Document Title:	**Improving Sex Estimation from Crania using 3-dimensional CT Scans**
Author(s):	**Richard L. Jantz, Mohamed Mahfouz, Natalie R. Shirley, Emam Abdel Fatah**
Document No.:	**240688**
Date Received:	**January 2013**
Award Number:	**2008-DN-BX-K182**

This report has not been published by the U.S. Department of Justice. To provide better customer service, NCJRS has made this Federally-funded grant report available electronically.

FINAL TECHNICAL REPORT

Improving Sex Estimation from Crania using 3-dimensional CT Scans

Award Number 2008-DN-BX-K182

Principal Investigator: Richard L. Jantz
University of Tennessee Anthropology Department

Co-Principal Investigator: Mohamed Mahfouz
University of Tennessee Department of Mechanical, Aerospace, & Biomedical Engineering

Postdoctoral Researcher: Natalie R. Shirley
University of Tennessee Anthropology Department

Graduate Student Researcher: Emam Abdel Fatah
University of Tennessee Department of Mechanical, Aerospace, & Biomedical Engineering

Abstract

Estimating sex of human crania has been traditionally, and remains, almost exclusively based on measurements or observations of external cranial features. These methods seldom exceed 90% accuracy and are often well below that. Since crania are over represented in forensic contexts, it is important to improve sexing accuracy from the cranium because sex is a foundational component of the biological profile (i.e. sex must be determined prior to establishing the remainder of the profile). This project utilizes an innovative approach to examine endo- and ectocranial measurements and obtain the best discriminators for sex estimation.

Three-dimensional skull models were constructed from computed tomography (CT) scans of crania from the William M. Bass Donated Collection housed at the University of Tennessee Anthropology Department (n=222, 141 males and 81 females). These models were used to create statistical bone atlases of the endo- and ectocranium. A bone atlas is a template that captures the primary shape variation in a skeletal element and allows for computer-automated measurements and shape analyses to be calculated rapidly from large datasets. An exploratory analysis of the principal components of the atlas was used to pinpoint areas of significant sexual dimorphism (we refer to this as the *global analysis*). Next, computerized linear and angular measurements were taken of each 3-D model to facilitate the *local analysis*. These craniometric measurements were a combination of select measurements from *Data Collection Procedures for Forensic Skeletal Material* (Moore-Jansen et al. 1994), measurements taken by Hsiao et al. (1996) from lateral radiographs, and several new measurements. Linear discriminant analysis with several variable selection procedures was used to evaluate the measurements and determine the most effective discriminators. Finally, the computer-automated measurements

were compared with manual measurements taken with calipers and (for the endocranial measurements) with measurements taken on lateral radiographs of a subset of the crania and tested for significant differences using a paired t-test (α=.05).

Results indicate that, while size is a significant component of cranial sex dimorphism, shape plays a role, as well. The global analysis showed significant size differences in cranial length and facial breadth and significant shape differences in the glabellar, zygomatic, occipital, and mastoid regions. The local analysis corroborated the global analysis. Important size-related variables that were captured by the discriminant analysis were bizygomatic breadth, maximum cranial length, cranial base length, and mastoid height. The shape-related variables appear to be capturing differences in the projection of the glabellar region, inclination of the frontal bone, and in the angulation/orientation of the mastoid. In addition, vault thickness is a sexually dimorphic feature, with females having on average thicker vaults than males in the frontal region, and males having thicker vaults in the occipital region (the former variable offered high discriminatory power). The best model is an 11-variable model that achieves 97.3%. It is also is possible to do well with only eight variables (95.5%), and three variables achieves 86.5% (IO-IOp, SN-SML, GPI). The glabella projection index (GPI) alone classifies with 82.4% accuracy, bizygomatic breadth (ZYB) achieves 83%, and basion-nasion length (BNL) 82%. The accuracy rates achieved in this study are higher than reported to date in the literature for the American population. Interestingly, the left side is consistently selected as a better classifier in the case of bilateral measurements, thus indicating the possibility of asymmetry in sexual dimorphism.

Table of Contents

List of Figures

List of Tables

Executive Summary

A. Research Problem and Goals

Estimating sex of human crania has been traditionally, and remains, almost exclusively based on measurements or observations of external cranial features. These methods seldom exceed 90% accuracy and are often well below that. Since crania are over-represented in forensic contexts, it is important to improve sexing accuracy because sex is an important component of the biological profile (i.e. sex must be determined before proceeding with the remaining elements of the profile: age, stature, and ancestry).

Studies by Hsiao et al. (1996), Rosas and Bastir (2002), and Franklin et al. (2004, 2005), found that measurements such as bizygomatic breadth and those capturing the size and shape of the glabellar region and the frontal bone are the most effective sex discriminators. We anticipate that angular measurements that quantify the frontal slope and angulation of the cranial base and occipital region will provide high discriminatory power. The purpose of the proposed research is to examine cranial sexual dimorphism in a modern American skeletal sample and provide criteria for sexing that improve success rates. The primary project goal is to provide practitioners with a set of cranial measurements (<10) that will achieve >90% accuracy and can be taken quickly and accurately on with calipers and on radiographs.

Briefly, three dimensional models developed from CT scans are used to construct statistical shape atlases of skeletal elements. An atlas uses coordinate data and iterative procedures to capture the primary shape variation in the bone and allows for computer-automated measurement extraction, landmarking, feature isolation, and the comparison of global shape differences across large datasets. The atlas has proven to be a powerful analytical tool, and this study expands its capabilities to investigate and quantify metric and geometric morphometric cranial sex dimorphism in a modern American sample and provide criteria for sexing that improve success rates. The analytical approach used in this study has been shown to improve sexing accuracy over traditional methods in postcranial bones, such as the patella and femur, and we hypothesize that we will have similar success with the cranium.

B. Research Design

The sample for this study is a subset of documented crania from people with 20th century birth years contained in the W. M. Bass Donated Skeletal Collection at the University of Tennessee's Department of Anthropology (n=222). The earliest birth year is 1903, the latest 1972 and the median birth year is 1937. The majority of the collection consists of American white individuals, so they will be the focus of the research. The computer algorithm for the statistical bone atlas does not handle fragmentary crania, crania missing bony elements, or irregularities in form between crania (i.e. varying numbers of teeth). Consequently partial, fragmentary or autopsied crania were omitted from this analysis, as was the dentition. This factor narrowed the sample size somewhat from the initial estimate; however, the study sample is sufficiently large. A separate sample of lateral radiographs of William M. Bass Donated Collection crania (n=30) was used to test if the computer measurements can be replicated accurately on radiographs.

Crania were scanned at 0.625mm slices and a resolution of 512 cubic voxels, and the resulting DICOM (Digital Imaging and Communications in Medicine) data sets were uploaded into the commercially available computer program Amira® for manual segmentation and model construction. For computational reasons, the models were simplified, reducing the number of faces to 100,000. Meshes are extracted from volumetric data segmentation and are usually manifold. Mesh quality includes the resolution of the mesh (number of faces and vertices), as well as the smoothness of the surface. The quality of template mesh can affect the landmark distribution in the atlas, and it can also cause washing out of landmarks. Different experiments were conducted to find the optimal mesh quality that guaranteed a smooth high resolution surface. For the skull mesh quality was chosen to be 25,000 vertices and 50,000 faces, for the ectocranial model this resolution preserves structure and landmarks with a reasonable processing time.

The next step is construction of the statistical bone atlas. A bone atlas is a template that captures the primary shape variation in a skeletal element and allows for computer-automated measurements and shape analyses to be calculated rapidly from large datasets. The input for this process is the segmented full skull surface meshes with no artifacts. The first step in the process is referred to as *mesh segmentation* which separates the skull into ecto- and endocranial surfaces. The ectocranial surface is then added to the atlas, and anatomical correspondence is generated. Next, the endocranial is referenced relative to the closest indices on the ectocranial atlas model. The two models are then joined again in a single model. An algorithm is used to create the statistical bone atlas, wherein the template mesh undergoes an iterative deformation process to match the bone to be added to the atlas and to generate anatomical correspondence across all vertices.

Deformation is the process of morphing the template model to match training model. This process determines the accuracy of correspondence, and thus blind deformation can lead to incorrect registration and point correspondence. In order to perform an accurate deformation, an initial registration step is required during which surface landmarks are matched based on surface shape properties. However, complex boney anatomy and the presence of noise can bias or affect the accuracy of registration process. In the perspective of this application noise is defined as any undesired components added from segmentation, model generation process, deformed anatomy or irregular bone growths. In order to overcome the effects of this problem, the most prominent surface features must be detected first. These features are used for the initial registration, and a matching step is performed followed by a weighted neighbor relaxation.

Two types of analyses were executed on the atlases: *global* and *local*. The global analysis examines the principal components of the statistical shape model to pinpoint areas of significant dimorphism. This analysis is a "feature-finding" step in that it detects morphological regions of high dimorphism that can be more carefully examined in the local analysis, as landmarks defined in these highly sexually dimorphic regions possess the best potential for sex determination. The local analysis uses endo- and ectocranial landmarks to compute geodesic measurements. Discriminant function analysis with stepwise variable selection is applied to these measurements to find the subset that gives the highest accuracy rates.

The global analysis was used to detect areas of high size and shape dimorphism. Size dimorphism was detected by applying Principal Components Analysis across all points in the atlas and examining the unscaled first principal component. Shape dimorphism was examined using a statistical treatment that combined Generalized Procrustes Analysis (GPA), Principal Components Analysis (PCA) and linear discriminant analysis (LDA) to detect areas of highest difference between the sexes. GPA calculates the atlas centroid and then translates it to the origin. This was done by taking *n* points, translating these points to the origin, and scaling them to the centroid size. Next, a rotation is calculated by minimizing the sum of squared distance between corresponding points in the atlas. After performing GPA to all models in the atlas, shape differences were extracted by using PCA. The resulting principal components consist of orthogonal eigenvectors that define a new set of coordinates with reduced dimensionality when the original features of the models are projected onto the eigenvectors scaled by the inverse of the singular values. These new coordinates were used to compare the differences between males and females by using Fisher's Discriminant Ratio to weight the PCA coordinates, and then summing the weighted vectors such that consistent differences between the two classes are retained. Fisher's Discriminant Ratio is the ratio of the between-class to within-class covariance matrices, and it is used frequently in pattern classification. The resulting vector magnitudes were reinterpreted as a 3-D deviation vector for each of the points on the models in the atlas. The deviation vector magnitudes were applied to a color map in order to visualize the areas of highest dimorphism. The most different areas are indicated by warm colors (red, orange, yellow) and the least different areas are indicated with cool colors (blues). The maxilla was omitted from the global analysis, as there was too much variation present among the models in this particular region, primarily because of edentulous individuals.

For the local analysis a set of predefined internal and external anatomical landmarks were automatically detected by utilizing skull geometry, curvature mapping and crest lines in order to get accurate measurements that reflect the actual skull dimensions. These landmarks were then used to calculate measurements of the internal and external cranial dimensions (see lists below). The measurements were calculated once on the atlas and then automated across all models in the atlas. Measurements were tested for significance discriminating capability using a measure of separation. Stepwise multilinear regression was used to determine the best variables to include in the discriminant model ($p \leq 0.1$ was used as the threshold for variables to be added during the regression). The selected variables were fed to a discriminant analysis classifier, and the classification percentage for each sex and total classification rate were calculated using leave-one-out cross-validation.

The following landmarks were located on the skull models:

1. *Basion*—most inferior posterior point in the midsagittal plane on the anterior rim of the foramen magnum.
2. *Gabella*—most anteriorly projecting point in the midsagittal plane at the lower margin of the frontal bone, which lies above the nasal root and between the superciliary arches
3. *Inion*—most prominent point of the external occipital protuberance
4. *Mastoidale*—lowest point of the mastoid process
5. *Metopion*—point where the line that connects the highest points of the frontal eminences crosses the sagittal plane
6. *Nasion*—the point of intersection of the naso-frontal suture and the midsagittal plane.
7. *Opisthocranion*—most posteriorly protruding point of the occipital bone in the midsagittal plane.
8. *Opisthion*—the point at which the midsagittal plane intersects the posterior margin of the foramen magnum.
9. *Porion*—midpoint of the external auditory meatus.
10. *Sella*—midpoint of the sella turcica.
11. *Supraglabella*—most posterior point in the midsagittal plane in the supraglabellar fossa; the concavity between glabella and metopion.
12. *Vertex*—the highest point on the cranial vault in the midsagittal plane (used in lieu of bregma on account of the absence of sutures in some of the models).
13. *Zygion*—the most laterally positioned point on the zygomatic arches

The following measurements were taken from these landmarks:

<u>Linear measurements (mm):</u>

1. Cranial base length (basion-nasion; BNL).

2. Maximum cranial length (glabella-opisthocranion; GOL).
3. Foramen magnum length (basion-opisthion; FOL).
4. Bizygomatic breadth (zygion-zygion; ZYB).
5. Mastoid height (porion to mastoidale, left and right; MDH).
6. Mastoid width—maximum width of the mastoid in the anterior-posterior direction.
7. Orbital height—greatest height of the orbit taken from points on the superior and inferior orbital margins (left and right; OBH).
8. Cranial height (vertex-basion; VB).
9. Frontal cord (vertex-nasion; VN).
10. Sella-Nasion (SN).
11. Sella-Basion (SB).
12. Mastoidale-Sella (left and right; MaS)
13. Mastoidale-Basion (left and right; MaB)
14. Glabella-Nasion (GN)
15. Glabella-Supraglabella (GSg)
16. Nasion-Supraglabella (NSg)
17. Glabella-Supraglabella-Nasion line—orthogonal distance from glabella to a line connecting supraglabella and nasion (G-SgN).
18. Glabellar projection index (GPI) = (glabella to supraglabella-nasion)*100/ (supraglabella to nasion).
19. Glabella superior-inferior projection index—a measure of the location of glabella along the midsagittal plane; G-SI-PI = GSg/GN.

<u>Angular measurements (°):</u>

20. Angle between the lines connecting glabella-metopion and sella-nasion (GM-SN).

21. Angle between the lines connecting glabella-metopion and basion-nasion (GM-BN).

22. Angle between the lines connecting glabella-sella and glabella-metopion (GS-GM).

23. Angle between the lines connecting inion-opisthocranion and sella-nasion (IOp-SN).

24. Angle between the lines connecting inion-opisthion and inion-opisthocranion (IO-IOp).

25. Angle between the lines connecting glabella-sella and glabella-nasion (GS-GN).

26. Angle between the lines connecting glabella-sella and sella-nasion (GS-SN).

27. Angle between the lines connecting sella-nasion and sella-mastoidale (right and left; SN-SMa).

28. Angle between the lines connecting inion-opisthion and basion-nasion (IO-BN).

29. Angle between the lines connecting inion-opisthocranion and basion-nasion (IOp-BN).

30. Angle between the lines connecting glabella-nasion and glabella-supraglabella (GN-GSg).

31. Mastoid angle—angle between the lines connecting mastoidale and the most anterior and posterior points where the mastoid contacts the cranial base (left and right; LMA and RMA).

32. Angle between the lines connecting sella-nasion and sella-mastoidale (right and left; SN-SMa).

<u>Thickness measurements (mm):</u>

33. Vault thickness at glabella (VTG).

34. Vault thickness at supraglabella (VTSg).

35. Vault thickness at metopion (VTM).

36. Vault thickness at opisthocranion (VTOp).

37. Vault thickness at inion (VTI).

38. Vault thickness at vertex (VTV).

In order to determine if the endocranial measurements obtained from the cranial atlas can be used in a lab without access to a CT scanner, subset of the Bass Collection crania (n=30) were used for a test study. Lateral x-rays were generated from the CT scans, and the radiographic measurements were taken with the freely available ImageJ software (http://rsbweb.nih.gov/ij/). In addition, the computer-automated ectocranial measurements were compared with measurements taken with calipers. Paired t-tests (α=.05) were used to test for significant differences between the two sets of measurements, and percent error was calculated to examine the magnitude of the differences.

$$\% \text{ error} = \frac{\left| \text{caliper or radiograph measurement} - \text{bone atlas measurement} \right|}{\text{bone atlas measurement}} * 100\%$$

C. Results and Conclusions

The results of the unstandardized PCA show that the first principal component (size) accounts for 35% of the variation in male crania and 41% in females. The first principal component is generally considered the percentage of variation attributed to differences in size. The first principal component shows that this variation is largely on account of differences in size of the glabellar region and cranial length, as well as mastoid size and facial breadth across the zygomatic bones. Principal components 2-10 account for an additional 38% of the variance in males and 34% in females. The second and third principal components are primarily capturing differences in the occipital region and in the zygoma, particularly the right zygomatic. The fourth principal component is showing differences in cranial breadth and in the zygoma, particularly the left zygomatic. Twenty principal components explain roughly 85% of the total variance, and 40 principal components account for 95%. Examined together PC1-40 highlight the differences in the glabellar region, zygomatics, and in cranial length. When the first principal component is removed, the shape differences in the glabellar region and in the zygoma are primarily apparent.

The results from the atlases with the GPA-PCA treatment to remove the effects of scale show that the first principal component picks up the differences in shape of the occipital region, they zygomatics (especially the right side) and cranial breadth. PC3 begins to pick up differences in the left zygomatic, while PC4 highlights the occipital differences again and brings in the glabellar region. Examining PC1-40 shows the differences in the shape of the glabellar region, and, to a lesser degree, in the inclination of the mastoid. Several of the targeted features are consistent with areas scored in nonmetric sex assessment (occiput/nuchal region, glabella, and mastoid).

The results of the local analysis include descriptive statistics and linear discriminant analysis. According to the separation index, the best discrimination variables involve glabella (GP-I and GN-GSg, both measures of glabellar projection) and traditional measurements bizygomatic breadth (ZYB), and cranial base length (BNL). Thereafter follow less traditional measurements glabellar projection index (GPI), GN-GSg angle, right and left mastoid to sella distances (MaS), GM-GS angle, sella to nasion (SN) and glabella-supraglabella (GSg). It should be noted that these are univariate statistics and do not necessarily predict which variables will enter a multivariate model. What they do show is what areas of the skull are most dimorphic, and these areas agree with those found in the global analysis. Face breadth has long been known to be a good discriminator, and ZYB alone discriminates with 81% accuracy in the present study. Beyond that we see that sagittal measurements are important (GOL, BNL, SN, GN-GSg), as well as the glabellar region and the mastoids. Again, these areas were all highlighted in the various principal components of the global analysis.

The model with the best classification results gets 97.3% accuracy with 11 variables (note: SN-SML cannot be measured on a radiograph). The next best model achieves 95.5% overall classification accuracy with just 8 variables, all of which are related to size differences. A model utilizing just shape variables (two angles and glabella projection index) classifies 86.5% of the cross-validated sample accurately; a model with variables capturing the shape of the brow ridge (GN-GSg and G-SgN) classifies 83.8% accurately. The glabella projection index alone gets 82%, as does basion-nasion length (cranial base length) and bizygomatic breadth (83%). With the exception of SN-SML, all of these measurements are taken easily with calipers and/or on a lateral or anterior-posterior radiograph. What is interesting is that vault thickness at metopion (VTM) always enters, despite having a relatively low univariate separation index. That is presumably because its sex dimorphism is opposite that of other direct measurements, females have larger values; VTM classifies alone at 69%.

This study has confirmed that, with respect to cranial sex dimorphism, size contributes a significant portion of the variation (35-41% of variance is explained by the first PC). However, shape is more important than was once thought. Important size-related variables that were captured in the discriminant functions were bizygomatic breadth (ZYB), maximum cranial length (GOL), and cranial base length (BNL). In addition, vault thickness is a sexually dimorphic feature, with females having on average thicker vaults than males. This was also documented by Ishida and Dodo (1990) and by Ross et al. (1998), who also found that female vault thickness increases with age, and male vault thickness decreases with age. Our results generally echo previous studies and support our predictions in that bizygomatic breadth, dimensions of the supraorbital region, and the occipital region are highly sexually dimorphic variables. While frontal bone morphology and bizygomatic breadth appear to typify sex dimorphism across populations (i.e. these variables are more universally dimorphic) (Franklin et al. 2004), there are population-specific aspects of sex dimorphism, as well.

As this study is an investigation of primarily non-traditional craniometrics (i.e. angles, endocranial measurements, and vault thickness), a limited number of overlapping measurements were available for comparing caliper measurements and virtual measurements: BNL, ZYB, FOL, GOL. MDH and OBH were not compared, as these measurements were calculated differently on the atlas. The Pearson correlation coefficients between the atlas and caliper measurements is high, but all measurements registered significantly different in the paired-t test of the means except FOL (foramen magnum length). Presumably this is because the hypothesized difference between the measurements is 0, thus making the paired t-test a highly sensitive measure of difference. However, the mean, median, and modal percent error is less than 1% in the majority of the measurements. Considering the sensitivity of the paired t-test as it was measured (hypothesized mean difference = 0), which does not allow for observer error, compared to the percent error calculations, we conclude that there is general agreement between manual and virtual measurements and between the virtual models and true cranial form.

A subset of the endocranial and angular measurements captured in the most accurate discriminant functions were taken from lateral radiographs. The measurements with the highest percent error are those containing sella, thereby suggesting the need for a more standardized method of locating this landmark on a radiograph. While some landmarks are easy to locate on radiographs (glabella, supraglabella, nasion), others are more difficult (sella, basion), and locating them accurately depends largely on the quality of the radiograph. Future research will work on refining the radiograph measurement definitions and protocols and reducing percent error.

D. Implications for Policy and Practice

One of the main components of the biological profile that forensic anthropologists develop from unidentified human skeletal remains is sex. It is well known, in the current state of the art, that postcranial elements are generally superior to cranial elements for sex estimation. Therefore, when cranial and postcranial elements are both present, forensic anthropologists typically give more weight to postcranial elements, especially os coxae. However, skeletal forensic cases often consist of a skull only, or a skull and fragmentary or incomplete postcranial remains. There do not appear to be concrete data concerning how frequently sex must be estimated solely from the cranium, either because it is the only element represented, or because the postcranial remains are too fragmentary to be useful. However, it is our experience at the University of Tennessee that crania are over represented in forensic casework. A query of the Forensic Anthropology Data Bank, which contains information submitted by forensic anthropologists around the country, revealed that skulls accompanied by specific postcranial elements are only about one-half as common as skulls without those elements. About 45% of skulls are unaccompanied by any sexable postcranial remains (i.e. a major long bone or os coxae). There is potential bias in these results in that skulls may be submitted to us for analysis without including postcranial remains, even though they may be present. There are, however, some reasons to accept the idea that crania are over represented in forensic casework:

- Crania are easily recognized as human by untrained observers, while postcranial elements are not as readily recognizable.
- Crania are less susceptible to carnivore damage than postcranial remains.

The success rate for sexing crania using traditional methods is 90% or less. Since the need to sex skeletal remains from the skull alone is a common occurrence, forensic anthropologists should have sexing criteria that are as reliable as possible. This study has provided a validated methodology for forensic anthropologists to estimate sex in modern Americans. Lateral radiographs are generally available to forensic anthropologists and, as shown here, introduce greater sexing accuracy into forensic practice without the need for expensive equipment or computer programs.

Finally, the American population is known to be changing rapidly, both demographically and morphologically. The William M. Bass Donated Collection is the largest and most well-documented collection of modern skeletons in the United States. It is no longer possible to rely on nineteenth century collections such as Terry and Hamann-Todd for forensic criteria. This study provides sexing criteria for modern Americans of European ancestry. More broadly, it has made the 3-D models of the crania available for access by anyone, thereby establishing the beginning of an online, virtual collection for cranial morphology that will have utility well beyond what is set forth in this project.

E. Implications for Further Research

This study was limited to Whites. It is obviously important to investigate other ancestries as well as other American and European populations. There is preliminary evidence from Fordisc that Whites are more dimorphic than Blacks who are more dimorphic than Hispanics. The general nature of variation in sex dimorphism variation should be investigated so there is a better understanding of where the greatest dimorphism is located in different populations.

Main Body of the Final Technical Report

I. Introduction

A. Statement of the Problem

Estimating sex of human crania has been traditionally, and remains, almost exclusively based on measurements or observations of external cranial features. These methods seldom exceed 90% accuracy and are often well below that. Since crania are over-represented in forensic contexts, it is important to improve sexing accuracy because sex is an important component of the biological profile (i.e. sex must be determined before proceeding with the remaining elements of the profile: age, stature, and ancestry). The purpose of the proposed research is to examine cranial sexual dimorphism in a modern American skeletal sample and provide criteria for sexing that improve success rates.

B. Review of the Literature

The literature dealing with sexing is extensive and spans many disciplines, including biological anthropology, archeology, biomedical engineering, odontology, and the forensic sciences. For sexing the skull, biological anthropologists have relied historically on visual assessment of features exhibiting obvious dimorphism. These features include brow ridges, mastoid size, supraorbital margins, chin morphology, and nuchal crest size (Komar and Buikstra 2008). Evaluation of these traits is subjective and to a considerable extent experience-based. Blind tests by experienced observers seldom yield accuracy in excess of 90%. Stewart (1979) achieved a success rate of 77% on Terry collection crania and Krogman (1962) managed 92% on the Todd collection, although he considered that an overestimate because males greatly outnumbered females. Recent work using modern samples of white Americans yielded correct assessments ranging between 89 and 92% (Williams and Rogers 2006; Rogers 2005). Treating the observations quantitatively reduces subjectivity somewhat, but does not improve accuracy appreciably (Konigsberg and Hens 1998). Walker (2008) has provided the most extensive analysis of traditional morphological features, including nuchal crest, mastoid process, orbital margin, glabella supraorbital ridge, and mental eminence. Even with standardized, multi-state scoring of traits and sophisticated statistical analysis, Walker could only achieve 88% correct classification of sex. This compares unfavorably with the nearly all postcranial elements which routinely provide sexing accuracy in excess of 90% (Spradley and Jantz 2011) Garvin and Ruff (2012) developed a method using laser scans for quantifying supraorbital form which is superior to the ordinal scoring system, but it did not improve sexing accuracy significantly. Reversing the usual situation, Ramsthaler et al. (2010) showed that CT scans could be used to score traditional traits in the absence of actual skeletal collections.

Metric sexing of crania using statistical procedures came to forensic anthropology via Giles and Elliott's (1963) classic paper, which presented sexing criteria for American whites and blacks from the Terry and Todd collections. Their success rate was in the high 80 percent, a rate typical of subsequent cranial sexing analyses. In general, it is rare to reach or exceed 90% correct sexing, whether one uses morphological traits or measurements. Uytterschaut (1986) achieved between 81% and 89% accuracy on Dutch, Zulu, and Japanese test samples using a discriminant function with four measurements (glabello-occipital length, bizygomatic breadth, nasal height and nasal breadth). Uytterschaut (1986) acknowledged that size variables are important in sex discrimination, but proposed that effectively isolating scale may yield accurate discrimination, as well. In one study, metric analysis found that bizygomatic breadth was the best single trait for sex discrimination in the cranium, achieving 80% in South African Blacks (Steyn and Iscan

1998). The results increased to 86% discrimination when five cranial measurements were included. Recent studies on sexing South African crania have provided similar accuracy rates using traditional and three-dimensional methods (Franklin et al. 2006, Dayal et al. 2008). Using 20th century Americans in the Forensic Anthropology Data Base from the University of Tennessee, correct assessment rates of 88-90% are commonly achieved (Komar and Buikstra 2008; France 1998). Likewise, recent analysis of the Greek population yielded 88 % (Kranioti et al. 2008).

While much of the research has focused on multiple cranial features and measurements, some research has focused on specific regions of the cranium, either in the hope they may provide simple, reliable sexing criteria, or because they may be necessary for sexing fragmentary crania. For example, an analysis of the sex differences in the supraorbital margin yielded 70% discrimination based on the gross morphology of this single indicator (Graw et al. 1999). Occipital condyles achieved 76 % (Gapert et al. 2009a) and foramen magnum only about 70 % (Gapert et al 2009b). Saini et al. (2012) achieved 87% with just two measurements in the mastoid area on an Indian sample.

Regardless of the number of morphological or metric traits considered, the traditional approaches described above rely on what can be observed subjectively or physically measured on the exterior of the skull. The ability to improve estimates in sexing using images and non-traditional measurements is suggested by a recent paper (Hsiao et al. 1996). These authors were able to classify 100% of a modern Taiwanese sample correctly by sex (50 males and 50 females), using measurements taken from lateral radiographs. This was accomplished by concentrating on the supraorbital ridges, frontal sinuses and nuchal crests. Males were found to have greater glabella projection and larger frontal sinuses. The greater male glabella projection is common knowledge, but it appears that measuring this feature precisely increases discrimination. These results were recently replicated on a French sample, where 95.6% accuracy was achieved (Veyre-Goulet et al. 2008), thereby illustrating the importance of frontal sinus and glabellar projection. Bigoni et al. (2010) also 99% - 100% correct sex classification on a known sex Central European sample using 3 dimensional coordinates, along with semi-landmarks quantifying curves midsagittal cranial shape.

Rosas and Bastir (2002) carried out a geometric morphometric analysis of sexual dimorphism using coordinate data to capture differences in shape. Their results also showed the importance of the supraorbital ridges and identified sexual dimorphism in angulation of the posterior cranial base, the occipital region, and the nasopharyngeal region. Additionally, they found three features of the mandible useful for sex diagnosis: curvature of the anterior symphysis, development of the pre-angular notch, and flexion of the ramus. According to these authors, size explained 53.7% of the total variance, and 37.3% of the variance could be attributed to the "sex specific factor," which they linked to differences between male and female skull anatomy not directly related to size. Rosas and Bastir (2002) assert that removing size in studies of cranial sex dimorphism is a way to eliminate its deceptive influence in sex discrimination. Another geometric morphometric analysis of cranial sex dimorphism in five modern South African populations from individuals in the Dart collection discovered certain features that distinguished males from females across all populations, including features of the frontal bone and zygomatic arches (Franklin et al., 2004). However, they also found features unique to certain populations and advocate analyses that take population variation into account. In a further geometric morphometry study limited to indigenous South Africans, Franklin et al. (2006) identified bizygomatic breadth, forehead contour profile, the form of the supramastoid crest, alveolar prognathism, and the size of the posterior airway space as the most dimorphic features. Franklin et al. (2005) tested the comparability of their 3-D coordinate data with traditional linear measurement data. They found that 3-D landmark coordinates can be transformed mathematically into 2-D linear measurements, thereby demonstrating the possibility of simultaneously collecting data for both types of studies with a digitizer or other instrument designed to collect coordinate data.

What emerges from Hsiao et al (1996), Rosas and Bastir (2002), and Franklin et al. (2004, 2005, 2006) and Lestrel et al. (2011) is the importance of shape in sexual dimorphism and improved performance using non-traditional features and innovative discovery methods. Over the past two years, our group has been able to improve sex estimation from post-cranial remains using 3-dimensional models from CT scans. We achieved classification success for patella sex determination using 3-D statistical shape models and nonlinear classifiers at a rate of 93.5% by testing classification with feed-forward back propagation Neural Networks (NN) (Mahfouz et al. 2007a). To date, traditional metric sexing had achieved only 85% from patellar measurements (Dayal and Bidmos 2005; Kemkes-Grottenthaler 2005). We created a femoral bone atlas that has proven valuable in recognizing sexual dimorphism at an extremely precise level, improving the reliability to sex the femur from 92% (Fordisc 3.0) to 95.4% using canonical variates analysis. By utilizing a newly developed statistical treatment that combines Principal Components Analysis (PCA) and the Fisher Discriminant Ratio (FDR), Mahfouz et al. (2007b) have been able to detect the most sexually dimorphic locations on the distal femur and explore how shape differences between the sexes change relative to size. Furthermore, an algorithm designed to detect bony landmarks automatically and propose measurements that most effectively capture the highest degree of sexual dimorphism promises to improve upon our ability to discriminate sex from skeletal remains using 3-D coordinate and/or linear measurement data (Mahfouz et al. 2007b).

Finally, much of the research on cranial sex discrimination in the American population has been carried out using anatomical collections containing individuals with 19th century birth years. It has been demonstrated that the American population has experienced considerable secular change in cranial morphology over the past 150 years (Jantz and Meadows Jantz 2000, Jantz 2001, Jantz and Wescott 2002), and these changes have been shown to affect ancestry estimation significantly (Ayres and Jantz 1990). However, the effect of secular change on sex estimation has not been examined systematically. Because it is at least possible, if not likely, that applying sex discrimination criteria based on 19th century crania will result in bias if applied to modern crania, further study in this area would prove beneficial to forensic anthropologists.

C. Statement of Hypothesis and Rationale for the Research

Based on studies such as those by Hsiao et al. (1996), Rosas and Bastir (2002), and Franklin et al. (2004, 2005), we expect to find that measurements such as bizygomatic breadth and those capturing the size and shape of the glabellar region and the frontal bone will prove to be the most effective discriminators of sex. Specifically, we anticipate that angular measurements that quantify the frontal slope, glabellar shape, and angulation of the cranial base and occipital region will provide high discriminatory power. The project goal is to provide practitioners with a set of cranial measurements (<10) that will achieve >90% accuracy and can be taken quickly and accurately with calipers and/or on a radiograph.

Briefly, three dimensional models developed from CT scans are used to construct statistical shape atlases of skeletal elements. An atlas uses coordinate data and iterative procedures to capture the primary shape variation in the bone and allows for computer-automated measurement extraction, landmarking, feature isolation, and the comparison of global shape differences across large datasets. The atlas has proven to be a powerful analytical tool, and this study expands its capabilities to investigate and quantify metric and geometric morphometric cranial sex dimorphism in a modern American sample and provide criteria for sexing that improve success rates. The analytical approach used in this study has been shown to improve sexing accuracy over traditional methods in postcranial bones, such as the patella and femur, and we hypothesize that we will have similar success with the cranium.

II. Methods

A. Study Sample

The sample for this study is a subset of documented crania from people with 20th century birth years contained in the W. M. Bass Donated Skeletal Collection at the University of Tennessee's Department of Anthropology (n=222). The earliest birth year is 1903, the latest 1972 and the median birth year is 1937. Started in 1981, this collection now has over 850 skeletons and is currently growing at the rate of about 100 skeletons per year. At the time of data collection during Year 1 of this project, the collection had approximately 650 crania available for CT scanning (shows the demographic composition of the collection). It is apparent that the majority of the collection consists of American white individuals, so they will be the focus of the research. The computer algorithm for the statistical bone atlas does not handle fragmentary crania, crania missing bony elements, or irregularities in form between crania (such as differences in the dentition—i.e. missing dentition). Consequently partial, fragmentary or autopsied crania were omitted from this analysis, as was the dentition. This factor narrowed the sample size somewhat from the initial estimate; however, the study sample is sufficiently large.

A separate sample of lateral radiographs of William M. Bass Donated Collection crania (n=30) was used to test if the computer measurements can be replicated accurately on radiographs.

Figure 1 Demographic composition of the Bass Donated Collection by percentage.

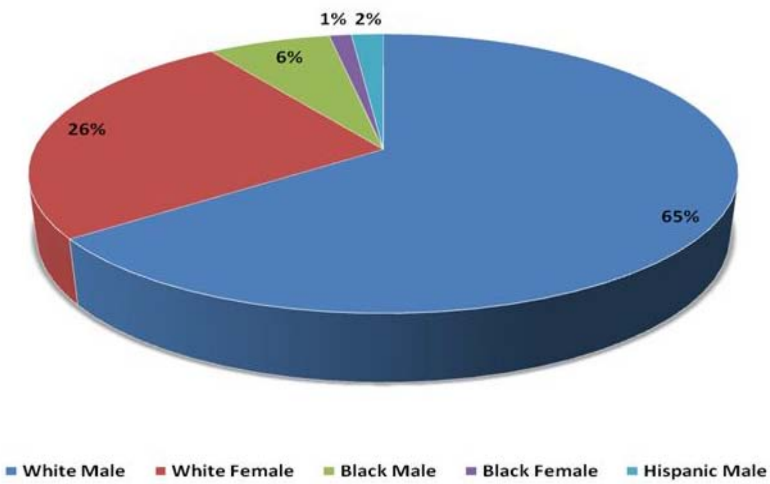

B. Medical Image Segmentation and Three-dimensional Model Construction

Crania were scanned using 0.625mm slices and a resolution of 512 cubic voxels, and the resulting DICOM (Digital Imaging and Communications in Medicine) data sets were uploaded into the commercially available computer program Amira® for segmentation and model construction. Initially, the DICOMs from the scanned crania were auto-segmented using MATLAB software. However, as some crania are left at the Anthropology Research Facility for >1 year prior to processing (either on the surface or buried) a large amount of variation was present in the preservation and density of the cranial bones (specifically the thin bones of the facial skeleton and bones with air sinuses). Consequently, automated thresholding and segmentation was abandoned for manual methods.

Segmentation of medical images is the process of dividing image data into contiguous regions that represent individual anatomical structures based on a specific set of criteria. Image segmentation was performed with Amira. Manual image segmentation begins by uploading a series of images into the Amira program. The user examines a single CT slice and selects regions of the slice that represent the anatomical structure of interest. Amira provides numerous tools for selecting the region of interest; we use maximum and minimum threshold grayscale values as criteria. By selecting grayscale values, any voxels that fall between the two threshold values are selected. Different voxel gray values correspond to different densities of sensed data. Cortical bone, being very dense, appears in a CT scan as having a very high voxel value (represented as white). Trabecular bone, with its relatively lesser density, appears gray, and thus has a lesser voxel value. Amira allows the periphery of each selected region (external and internal) to be captured as a continuous colored line termed a 'label.' Additional labels can be created for different structures. The user repeats the process for each slice that contains the structure of interest, altering the threshold values that best capture the structure in a specific slice. Once each slice has been segmented, a 3-D model of the structure can be generated; Amira stacks the labels and interpolates between them to compile a three-dimensional surface model with approximately 2,000,000 faces (Figure 2). For computational reasons, the models were simplified, reducing the number of faces to 100,000.

Figure 2. Segmented sagittal section (left) and 3-D surface model generated from contiguous labels (right).

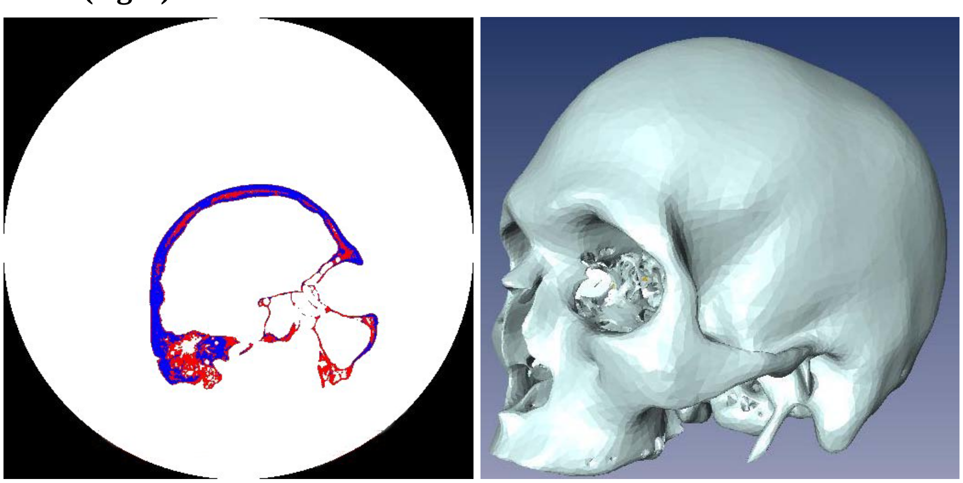

C. Mesh Artifacts

Meshes are extracted from volumetric data segmentation and are usually manifold. Mesh upon triangulation of volumetric data is usually in the range of 1.5 million faces. Processing such a large number of faces and vertices would be costly, and thus models have to be decimated to lower the number of triangles and then smoothed. However, the existence of porous boney areas (small areas with low bone quality) can generate artifacts in output mesh such as spurious handles, disconnected components, duplicate vertices, and cavities. These artifacts can affect the quality of the registration algorithm and thus a preprocessing step is required to fix any model degeneracy. Figure 3 shows flow chart of detecting artifacts and fixing model degeneracy.

Figure 4 shows an example of the input skull mesh, detected degeneracy, and the fixed output mesh.

Figure 3. Fixing mesh degeneracy.

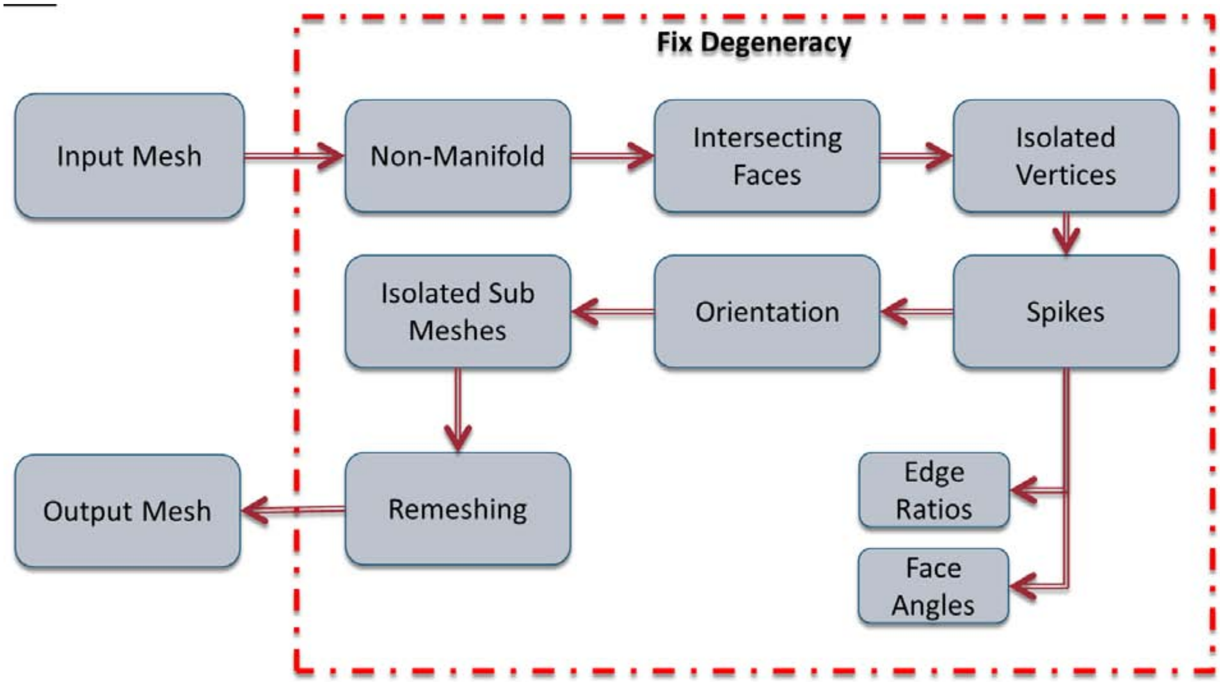

Figure 4. Input mesh, detected degeneracy and output mesh.

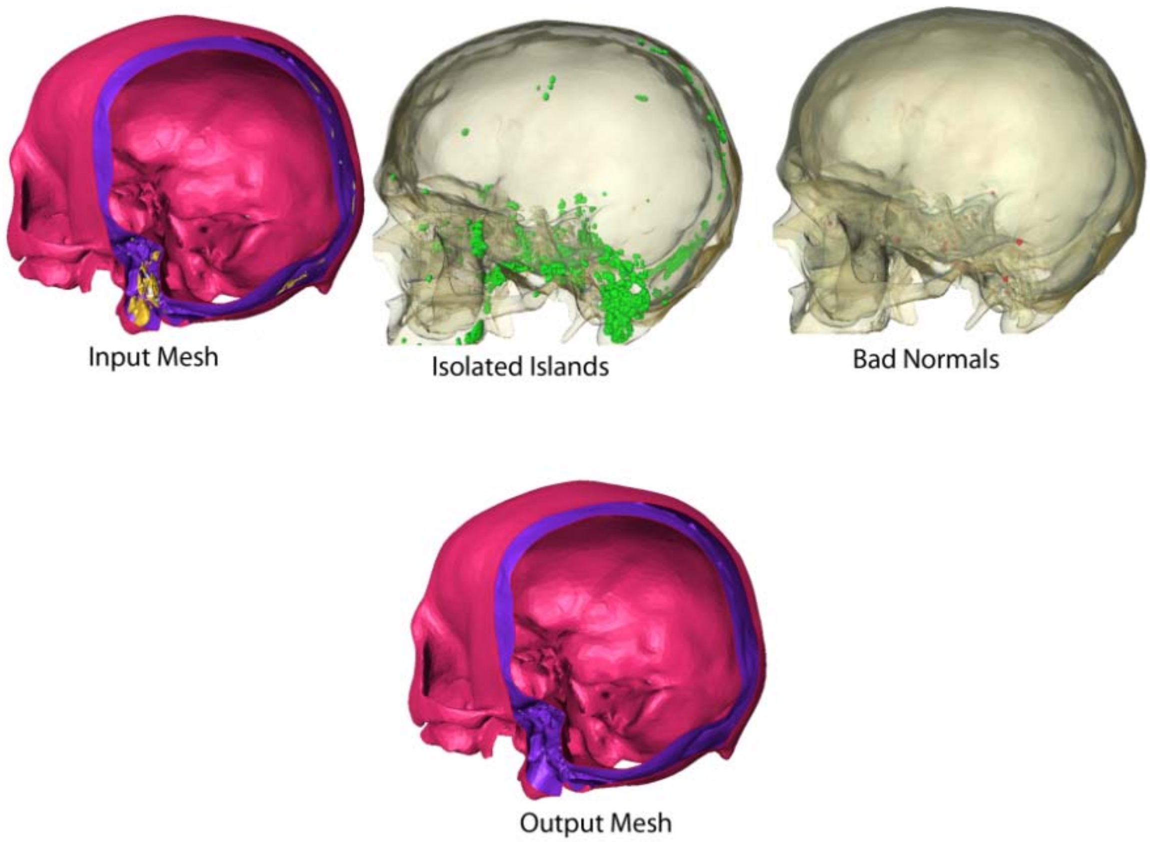

C.1. Template Mesh Quality

Mesh quality includes the resolution of the mesh (number of faces and vertices, Figure 5) as well as the smoothness of the surface. The quality of template mesh can affect the landmark distribution in the atlas, and it can also cause washing out of landmarks. Figure 6 shows the effect of mesh quality on the accuracy of calculated landmark. Different experiments were conducted to find the optimal mesh quality that guaranteed a smooth high resolution surface. For the skull mesh quality was chosen to be 25,000 vertices and 50,000 faces for the ectocranial model; this resolution preserves structure and landmarks with a reasonable processing time.

Figure 5 Mesh quality as a measure of different triangle resolution.

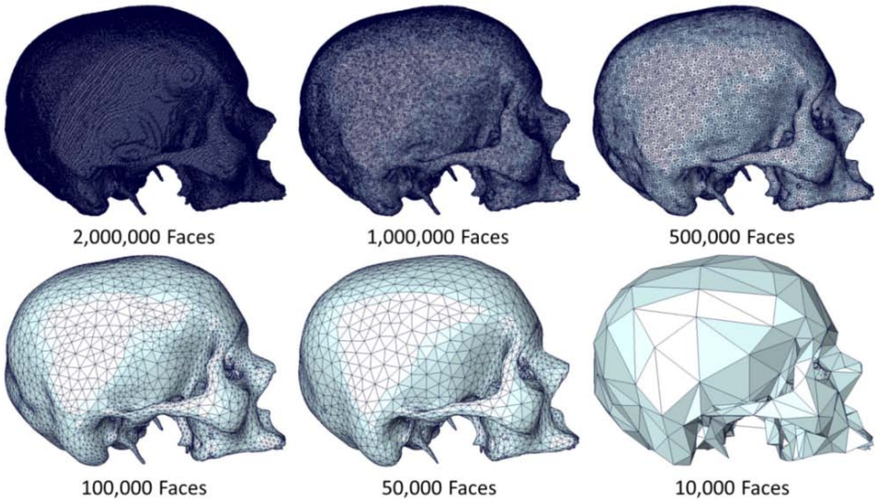

Figure 6 Effect of mesh quality on landmarks.

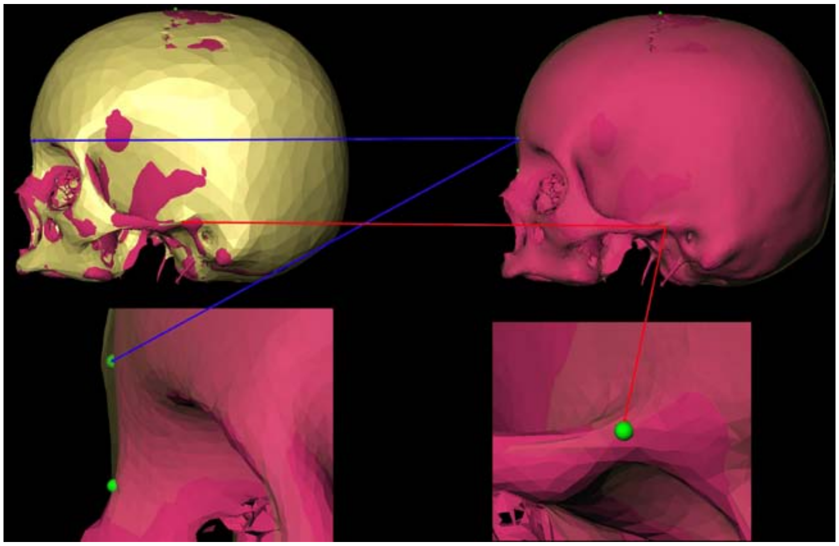

D. Skull Atlas

Figure 7 outlines the process of creating the skull atlas. A bone atlas is a template that captures the primary shape variation in a skeletal element and allows for computer-automated measurements and shape analyses to be calculated rapidly from large datasets. The input for this process is the segmented full skull surface meshes with no artifacts. The first step in the process is referred to as *mesh segmentation* which separates the skull into ecto- and endocranial surfaces. The ectocranial surface is then added to the atlas, and anatomical correspondence is generated.

Next, the endocranial is referenced relative to the closest indices on the ectocranial atlas model. The two models are then joined again in a single model.

Figure 7. Process of skull atlas creation.

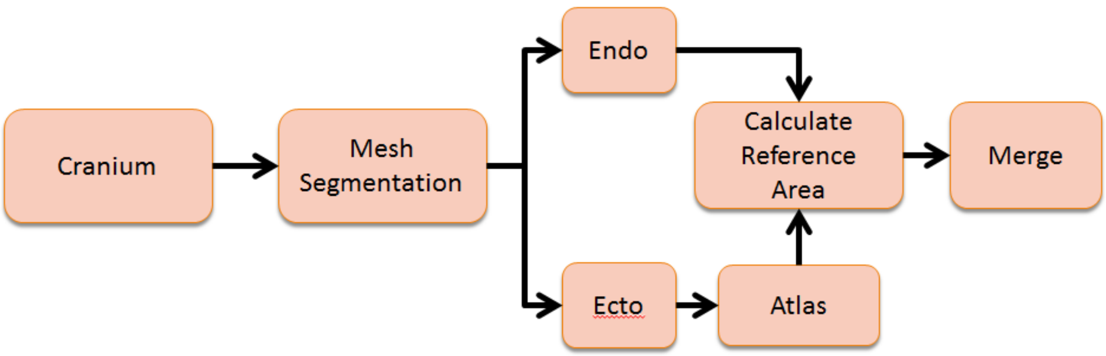

D.1. Mesh Segmentation

The cranium is a complex structure with many ectocranial and endocranial features. However, greater inconsistency exists in the more delicate endocranial features as a result of the variation in postmortem bone quality (Figure 8). In turn, this variation increases the error from segmentation process, which can introduce error in the atlas creation process. Consequently, to minimize error in the statistical atlas, the cranium was separated into two components: ectocranial and endocranial surfaces. This created the need for a mesh segmentation technique that can perform this task efficiently and consistently.

Figure 8. Inconsistency in internal surface.

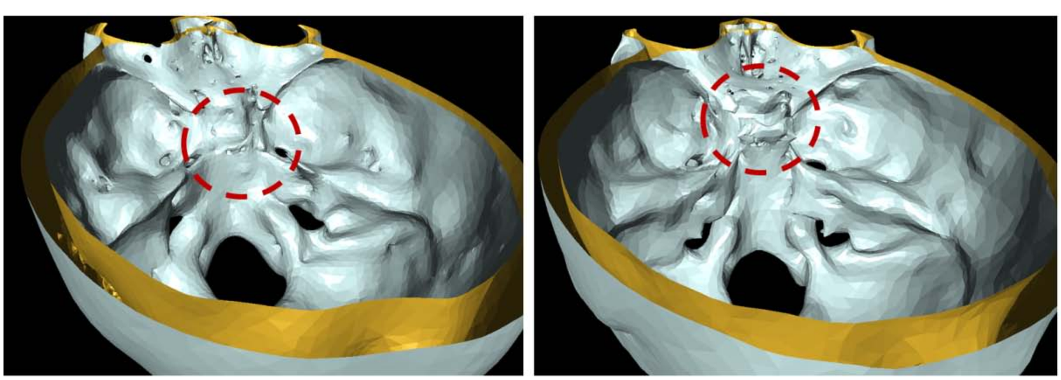

Mesh segmentation is the process of partitioning mesh into different components; it has become a key element in many geometric modeling and computer graphics applications. It aids the parameterization, deformation, editing, and shape matching (Shamir 2008). Methods developed for mesh segmentation utilize techniques from image processing and unsupervised machine learning. Different algorithms have been developed to perform mesh segmentation into meaningful constituent parts (Agathos et al. 2010) (Figure 9). However, all of these algorithms are general in the sense that they use features on the mesh for partitioning with no regard to the semantics of each segment.

Figure 9 Example of mesh segmentation.

A novel technique was developed to segment the skull mesh into ecto- and endocranial surfaces, and details of this algorithm are outlined in Figure 10.

Figure 10 Mesh segmentation algorithm

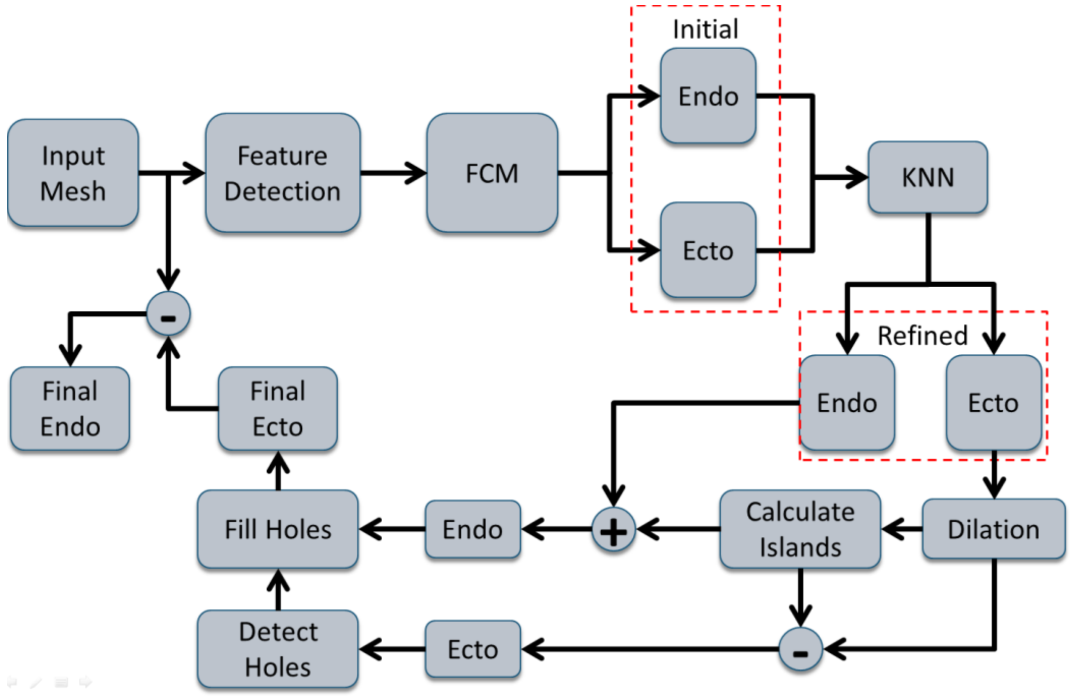

The algorithm starts first by calculating the following set of features from the input skull model (Figure 11):

1. Angle between centroid-Vertex vector and normal vector
2. Angle between centroid-Vertex vector and smoothed normal vector
3. Feature #1 of the first intersection point
4. Number of intersection points
5. Ratio between first intersection point-Vertex distance and last intersection point-Vertex

These features are then clustered using fuzzy c-means clustering (FCM) (Bishop 2006).

Minimize function: $E(U,V) = \sum_{i=1}^{k} \sum_{j=1}^{n} (u_{ij})^m \left\| \bar{x}_j - \bar{v}_i \right\|^2$

Subject to $\sum_{i=1}^{k} u_{ij} = 1 \qquad \forall j = 1, \dots, n$

Fuzzy partition matrix $U = \left[u_{ij} \right]_{k \times n} \qquad u_{ij} \in [0,1]$

Fuzzification parameter $m \in [1, \infty]$

Figure 11 Feature generation algorithm.

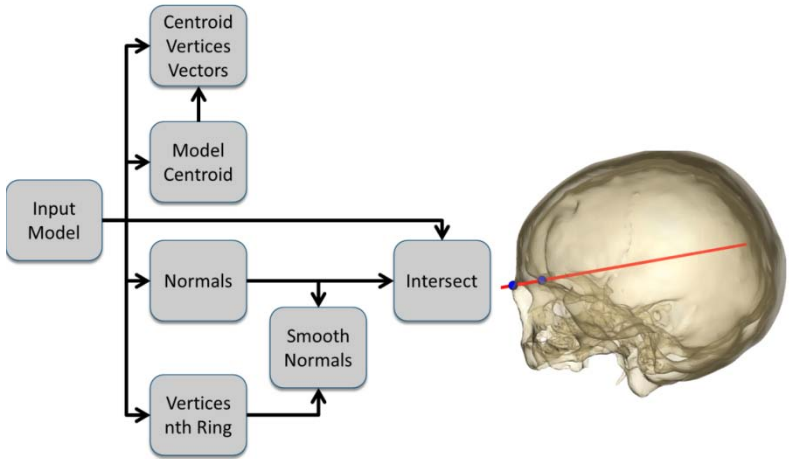

The output from FCM clustering provides an initial guess of the two clusters (Figure 12). A confidence score is then calculated for each point and used to remove outliers from each cluster. Next, a dilatation step is performed on the ectocranial points using 1 ring neighbors, and isolated vertices are then calculated from the ectocranial surface and added to the list of endocranial. The final step is to detect any holes in the ectocranial surface. These holes are then filled with closest points from endocranial surface.

Figure 13 shows the final segmented surfaces.

Figure 12 Evolution of ecto- and endocranial surface during segmentation process

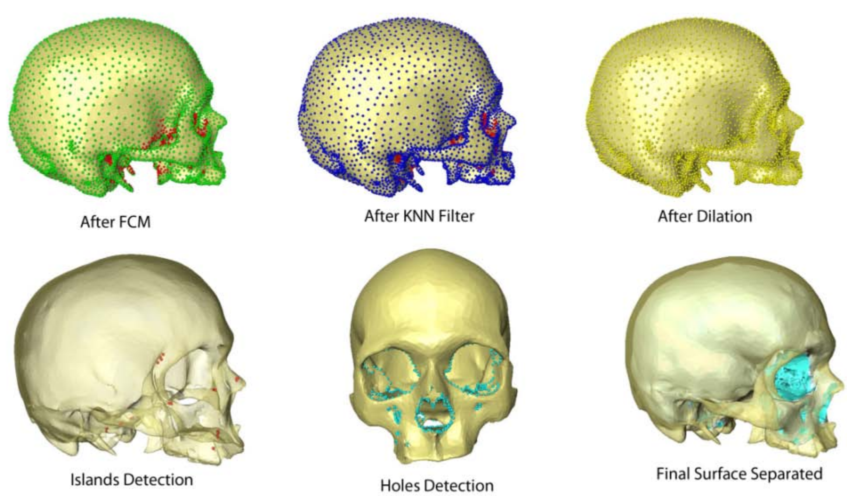

Figure 13 Final segmented ecto and endo cranial surfaces

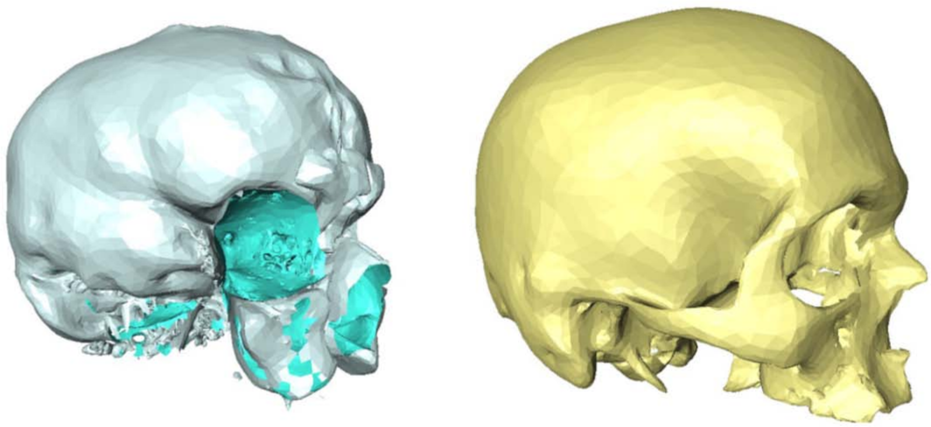

D.2. Atlas Creation

Error! Reference source not found. outlines the algorithm for the statistical bone atlas creation, where template mesh undergoes an iterative deformation process to match the bone to be added to the atlas and to generate anatomical correspondence across all vertices.

Figure 14 Atlas creation algorithm.

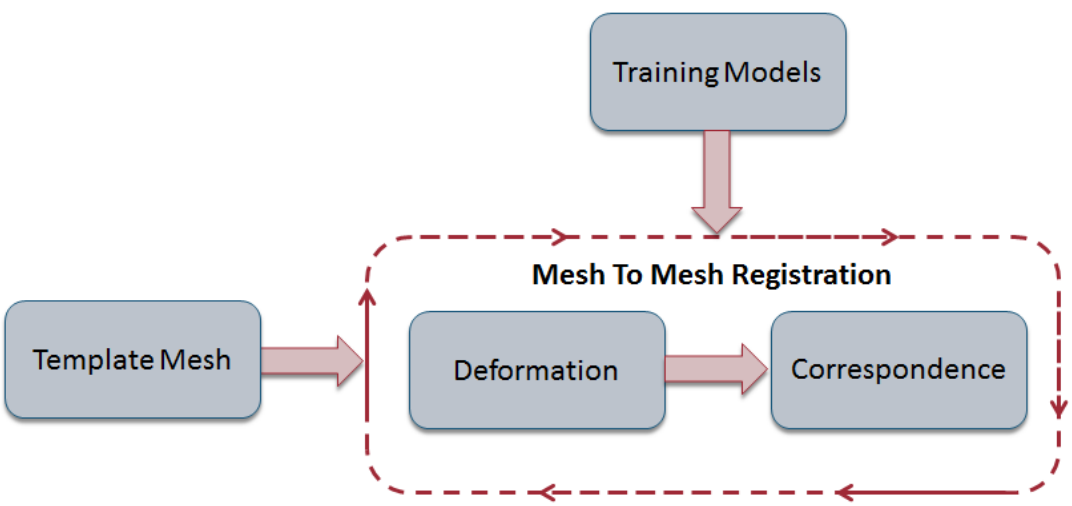

D.3. Deformation

Deformation is the process of morphing the template model to match training model. This process determines the accuracy of correspondence, and thus blind deformation can lead to incorrect registration and point correspondence. In order to perform an accurate deformation, an initial registration step is required during which surface landmarks are matched based on surface shape properties. However, complex boney anatomy and the presence of noise can bias or affect the accuracy of registration process. In the perspective of this application noise is defined as any undesired components added from segmentation, model generation process, deformed anatomy or irregular bone growths. In order to overcome the effects of this problem, the most prominent surface features must be detected first. These features are used for the initial registration, and a matching step is performed followed by a weighted neighbor relaxation. Figure 15 outlines the overall deformation process.

Figure 15 Deformation process.

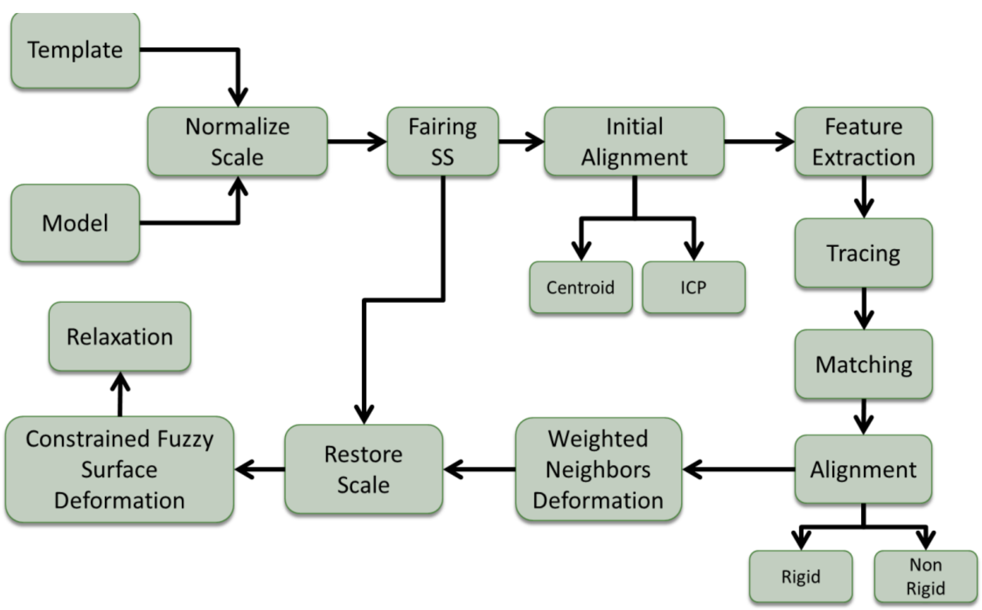

Figure 16 Template model and model to add in scale space.

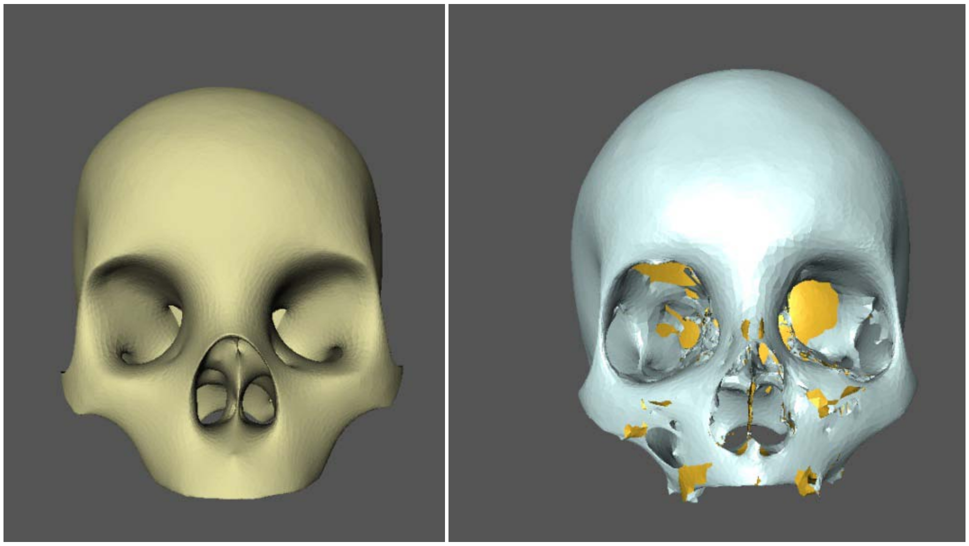

Figure 17 Template and new mesh to add after alignment

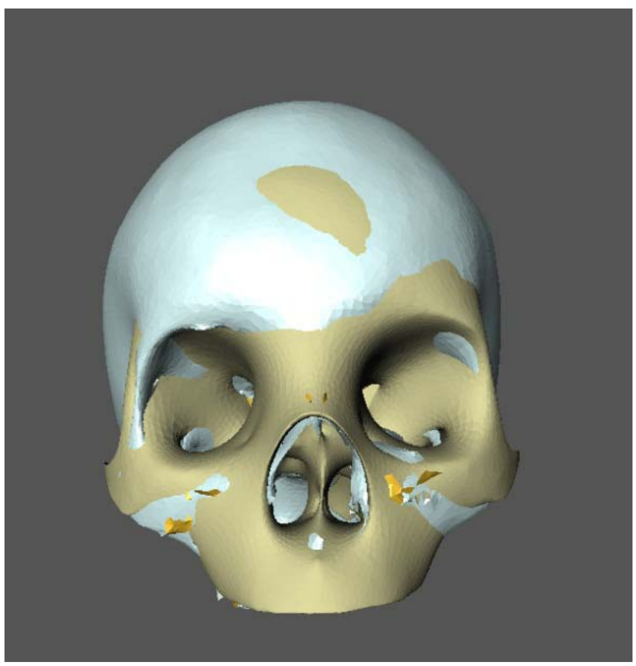

Figure 18 Feature points detected on template mesh.

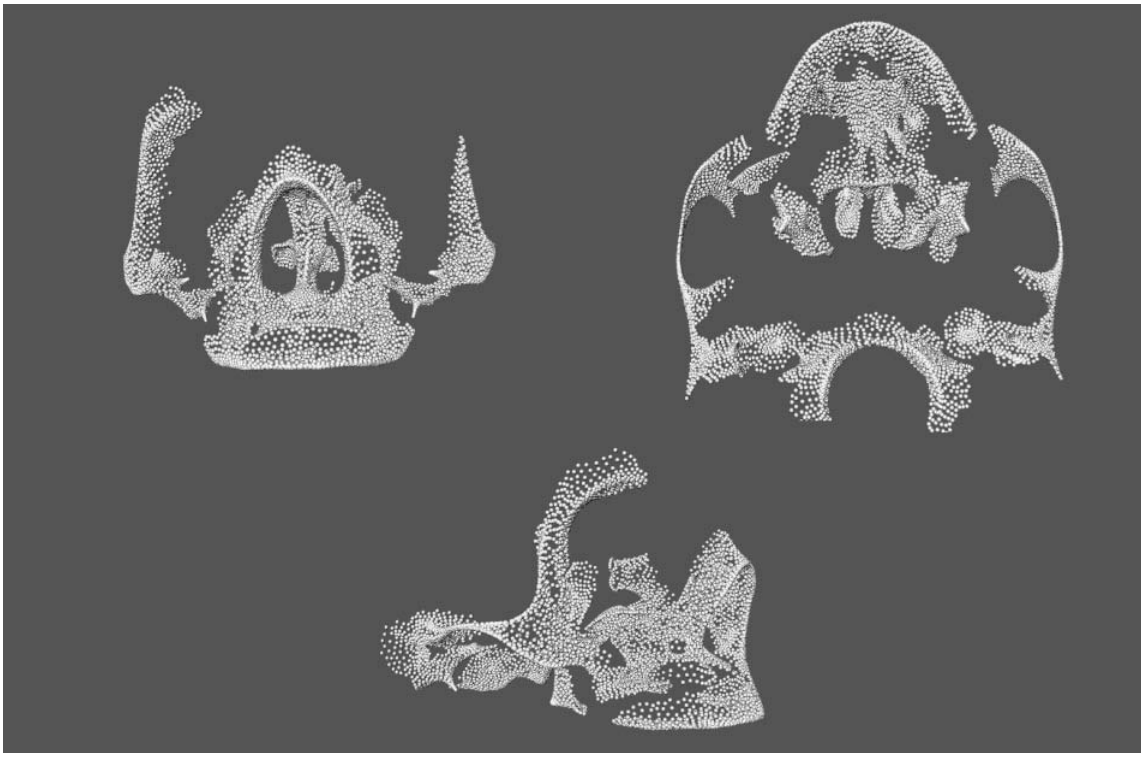

Figure 19 Feature points detected on new mesh to be added to atlas.

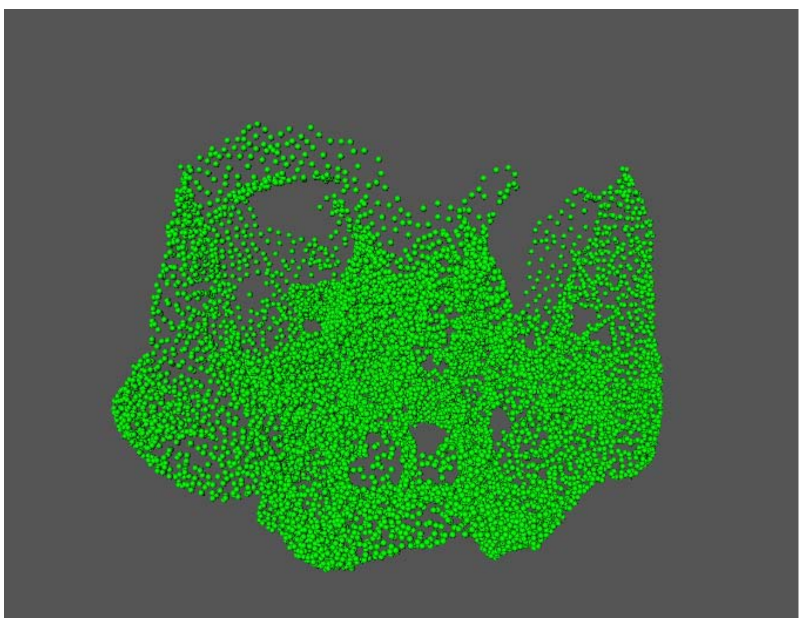

Figure 20 Matching and alignment of template feature (red) and mesh to add (green).

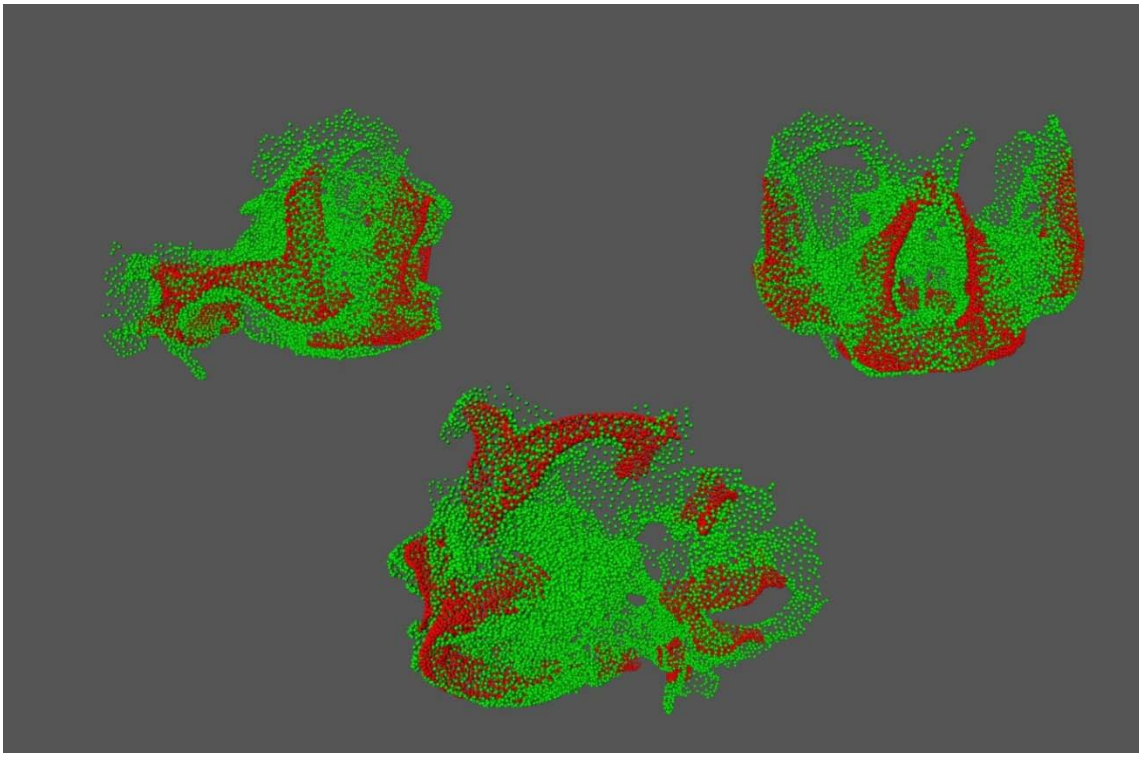

Figure 21 Template mesh after deformation (gold); model to add (cyan).

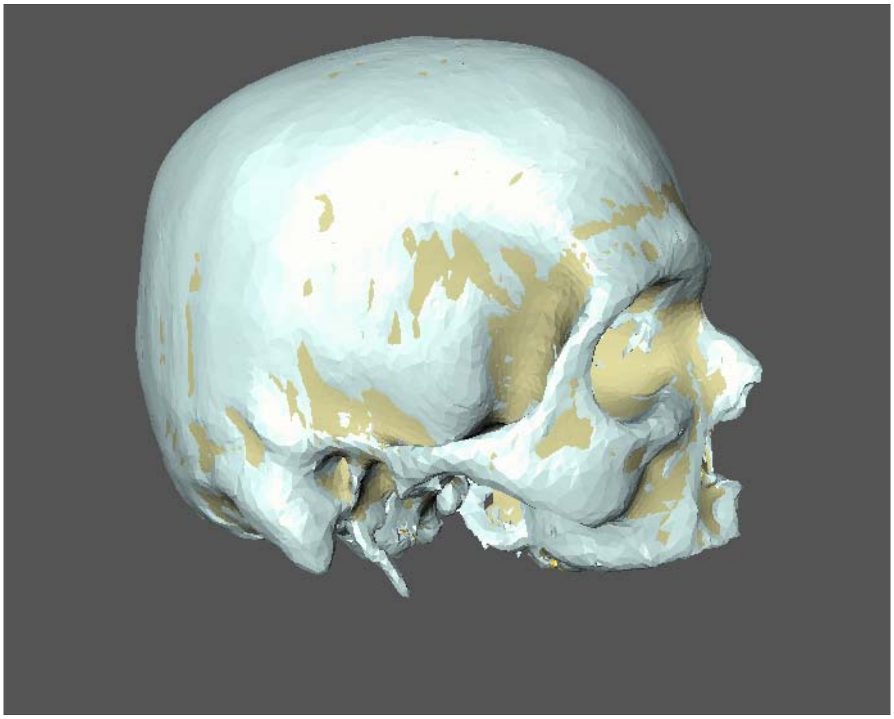

Figure 22 Final atlas model (Gold); original mesh to add (Cyan)

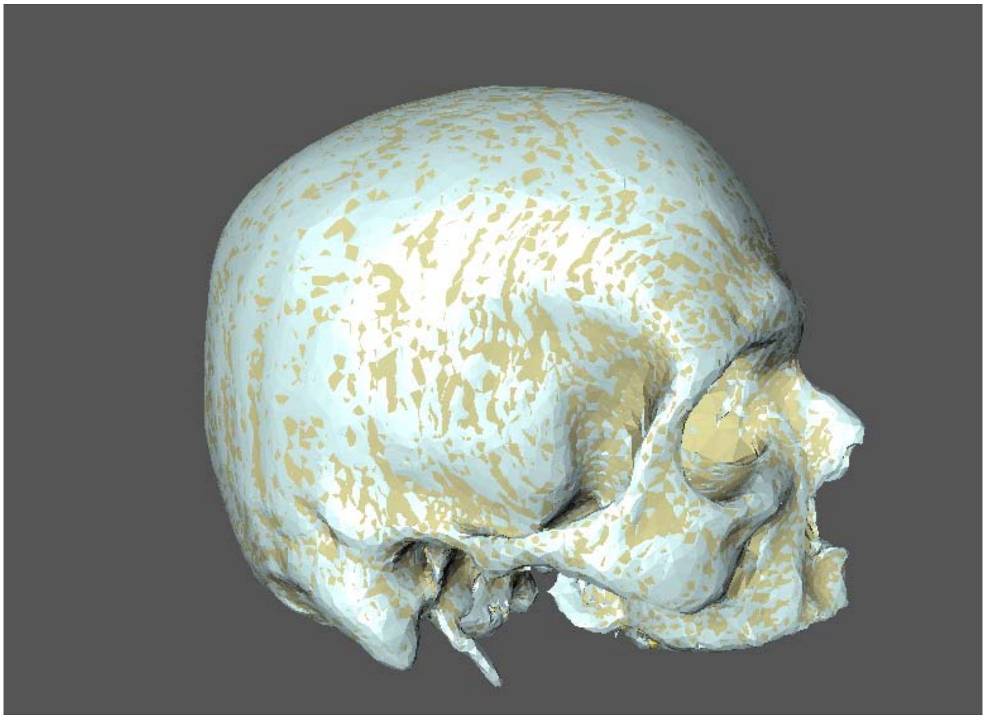

Figure 23 Distance error map (0 mm blue - 1 mm red).

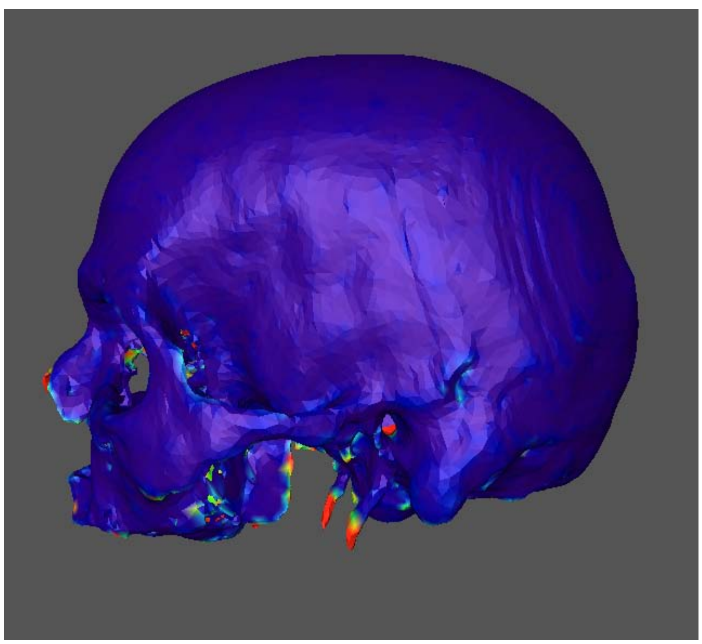

E. Global and Local Analyses

Two types of analyses were executed on the atlases: global and local. The global analysis examines the principal components of the statistical shape model to pinpoint areas of significant dimorphism. This analysis is a "feature-finding" step in that it detects morphological regions of high dimorphism that can be more carefully examined in the local analysis, as landmarks defined in these highly sexually dimorphic regions possess the best potential for sex determination. The local analysis uses endo- and ectocranial landmarks to compute geodesic measurements. Discriminant function analysis with stepwise variable selection is applied to these measurements to find the subset that gives the highest accuracy rates.

E.1. Global Analysis

The global analysis was used to detect areas of significant size and shape dimorphism. Size dimorphism was detected by applying Principal Components Analysis across all points in the atlas and examining the unscaled first principal component. Shape dimorphism was examined using a statistical treatment that combined Generalized Procrustes Analysis (GPA), Principal Components Analysis (PCA) and linear discriminant analysis (LDA) to detect areas of highest difference between the sexes. GPA calculates the atlas centroid and then translates it to the origin. This was done by taking n points, translating these points to the origin, and scaling them to the centroid size. Next, a rotation is calculated by minimizing the sum of squared distance between corresponding points in the atlas. After performing GPA to all models in the atlas, shape differences were extracted by using PCA. The resulting principal components consist of orthogonal eigenvectors that define a new set of coordinates with reduced dimensionality when the original features of the models are projected onto the eigenvectors scaled by the inverse of the singular values. These new coordinates were used to compare the differences between males and females by using Fisher's Discriminant Ratio to weight the PCA coordinates, and then summing the weighted vectors such that consistent differences between the two classes are retained. Fisher's Discriminant Ratio is the ratio of the between-class to within-class covariance matrices, and it is used frequently in pattern classification. The resulting vector magnitudes were reinterpreted as a 3-D deviation vector for each of the points on the models in the atlas. The deviation vector magnitudes were applied to a color map in order to visualize the areas of highest dimorphism. The most different areas are indicated by warm colors (red, orange, yellow) and the least different areas are indicated with cool colors (blues). The maxilla was omitted from the global analysis, as there was too much variation present among the models in this particular region as a result of the cutoff points for omitting the dentition.

E.2. Local Analysis: Landmarking and linear/angular measurements

For the local analysis a set of predefined internal and external anatomical landmarks were automatically detected by utilizing skull geometry, curvature mapping and crest lines in order to get accurate measurements that reflect the actual skull dimensions. These landmarks were then used to calculate measurements of the internal and external cranial dimensions. The process of automatic landmarking utilizes both the ability of the atlas to propagate anatomical correspondence across population and thus define landmark loci, as well as mathematical and geometrical constraints to calculate the landmarks on each bone as shown in Figure 24.

Figure 24 General framework of automatic landmarking.

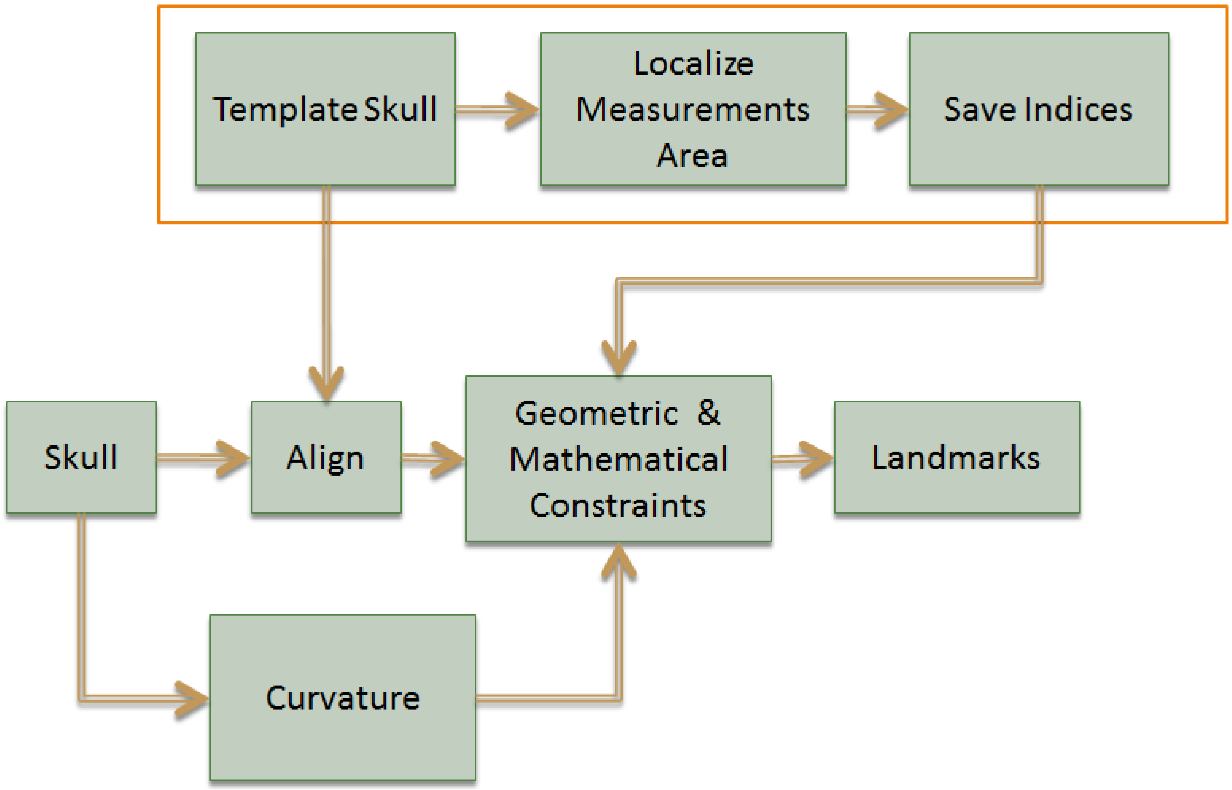

Figure 25 Landmark calculation.

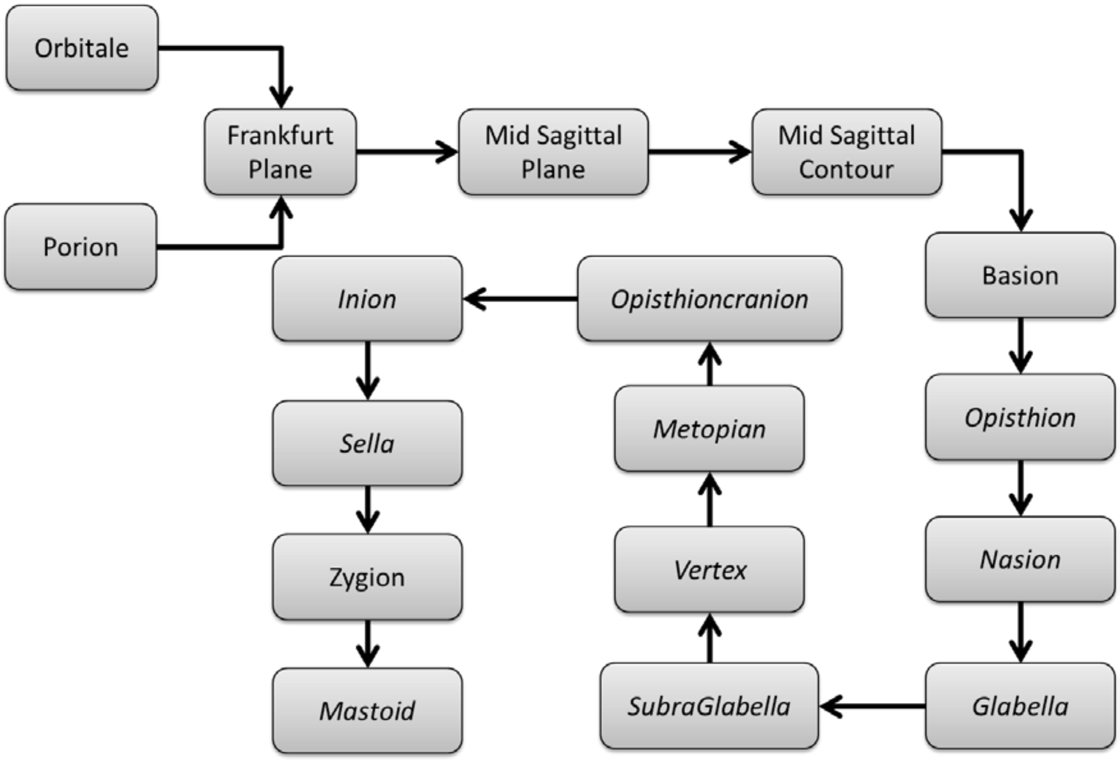

Figure 26 Left orbitale (Top: purple dot) and porion (Bottom: green dot on right and blue dot on left)

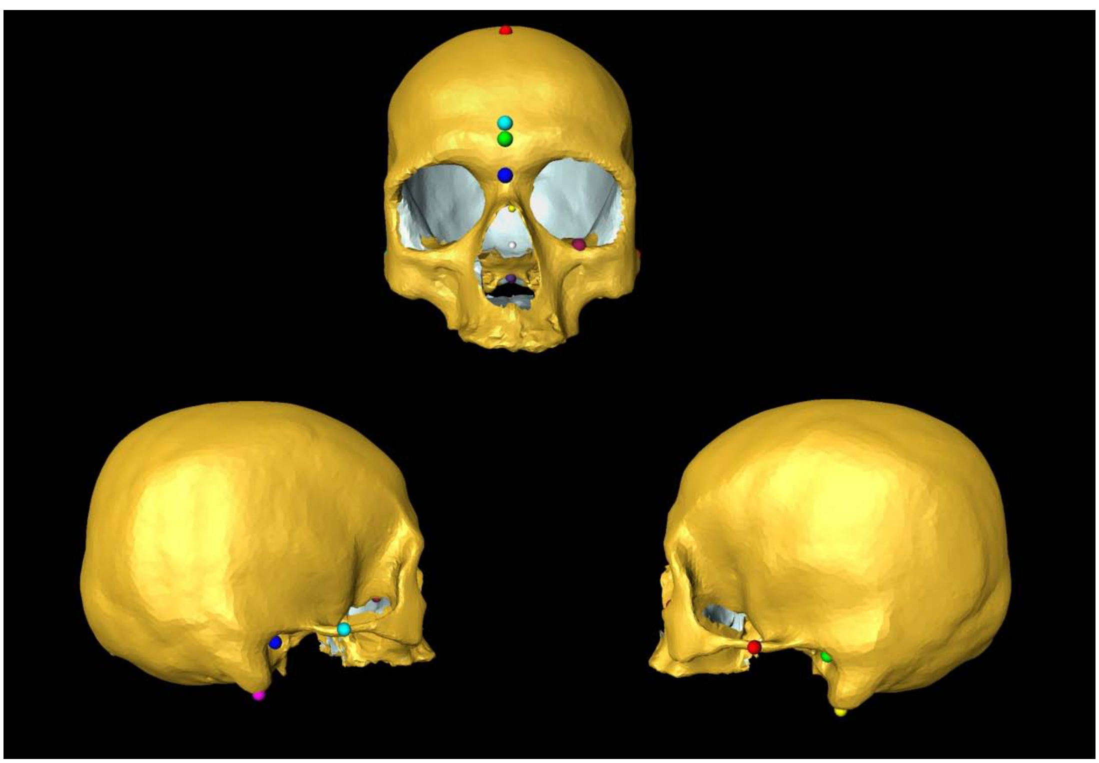

Figure 27 Frankfurt plane defined as plane passing through left, right porion and left orbitale. Midsagittal plane defined as normal to Frankfurt Horizontal plane and passing through bone centroid.

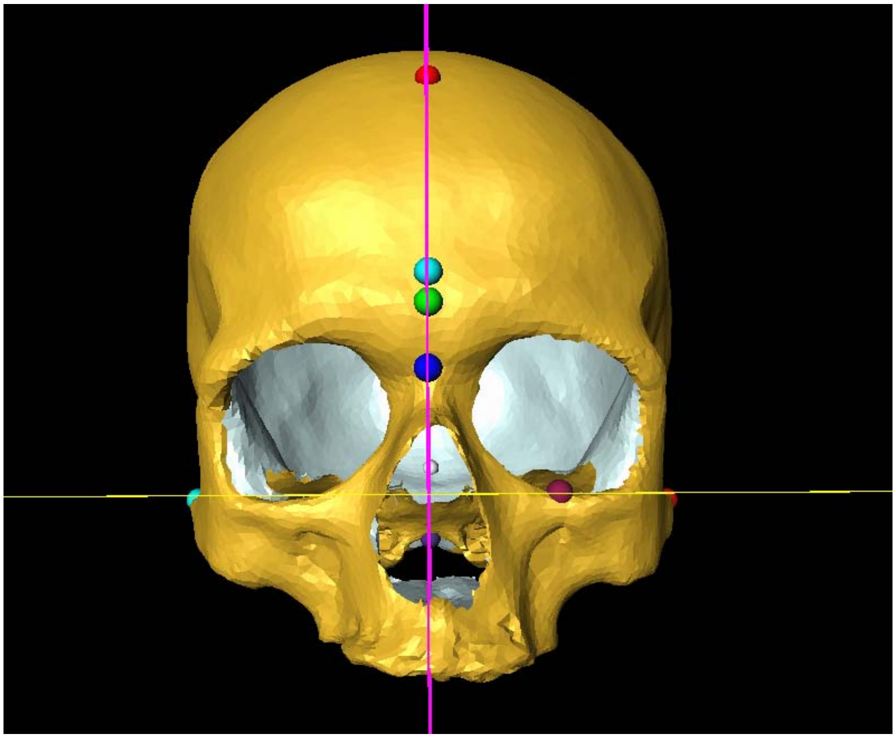

Figure 28 Lateral view of Frankfurt plane defined as plane passing through left, right porion and left orbitale and midsagittal plane defined as normal to Frankfurt Horizontal plane and passing through bone centroid.

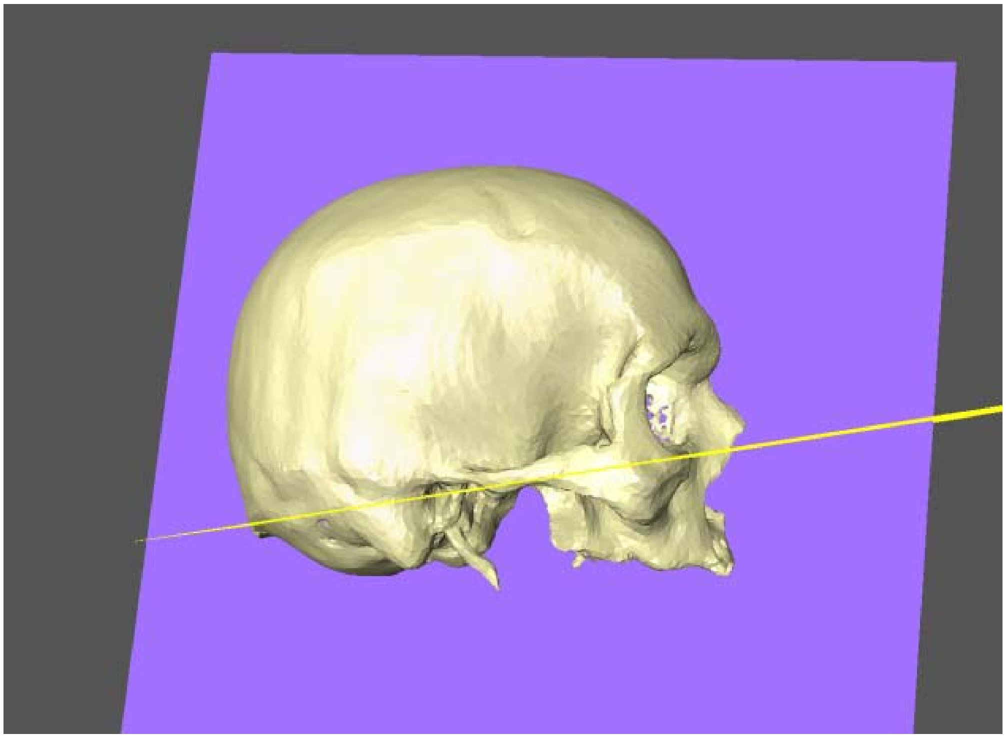

Figure 28 Skull intersection with midsagittal plane.

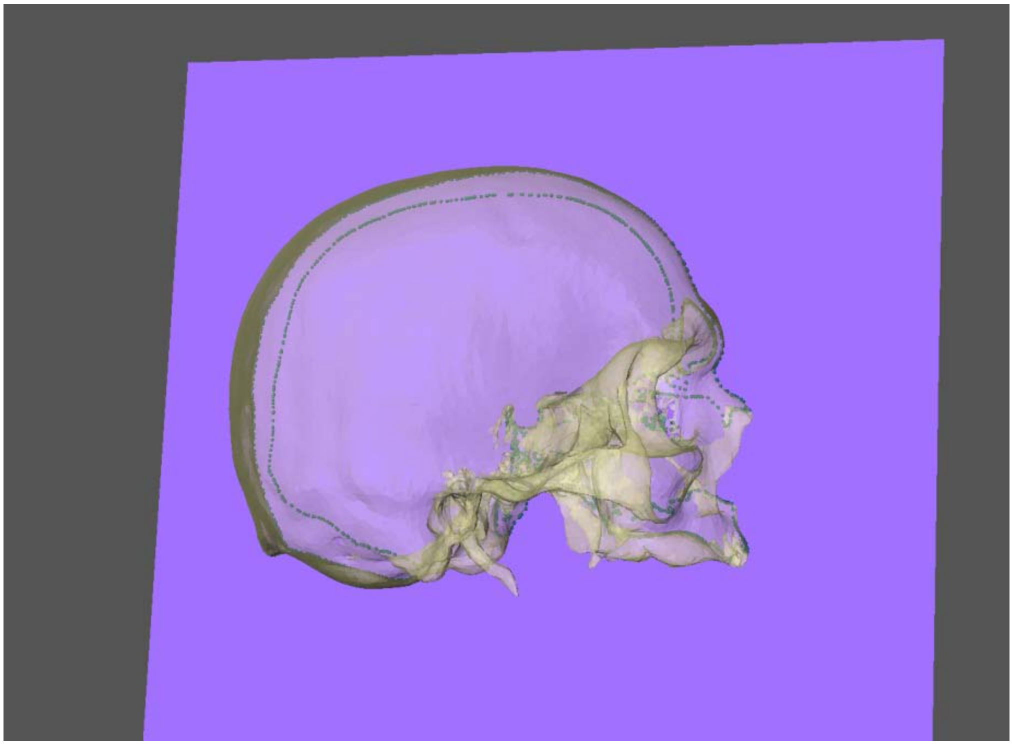

Figure 29 Extracted midsagittal contour.

Figure 30 Calculated landmarks on midsagittal contour.

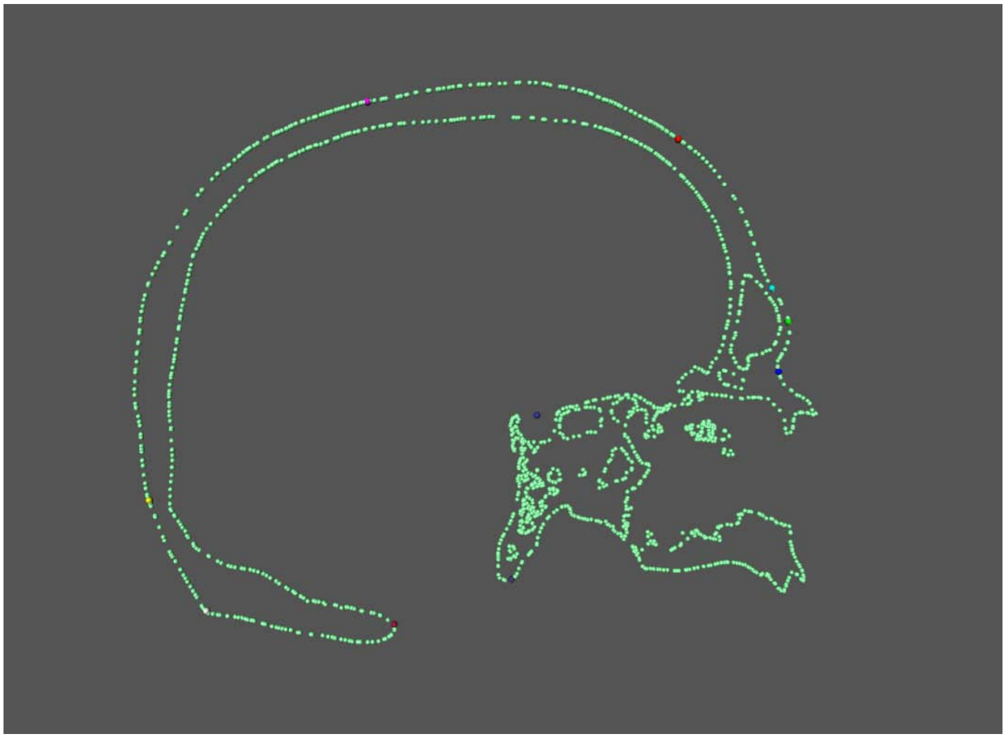

Figure 31 Left zygion and left mastoid.

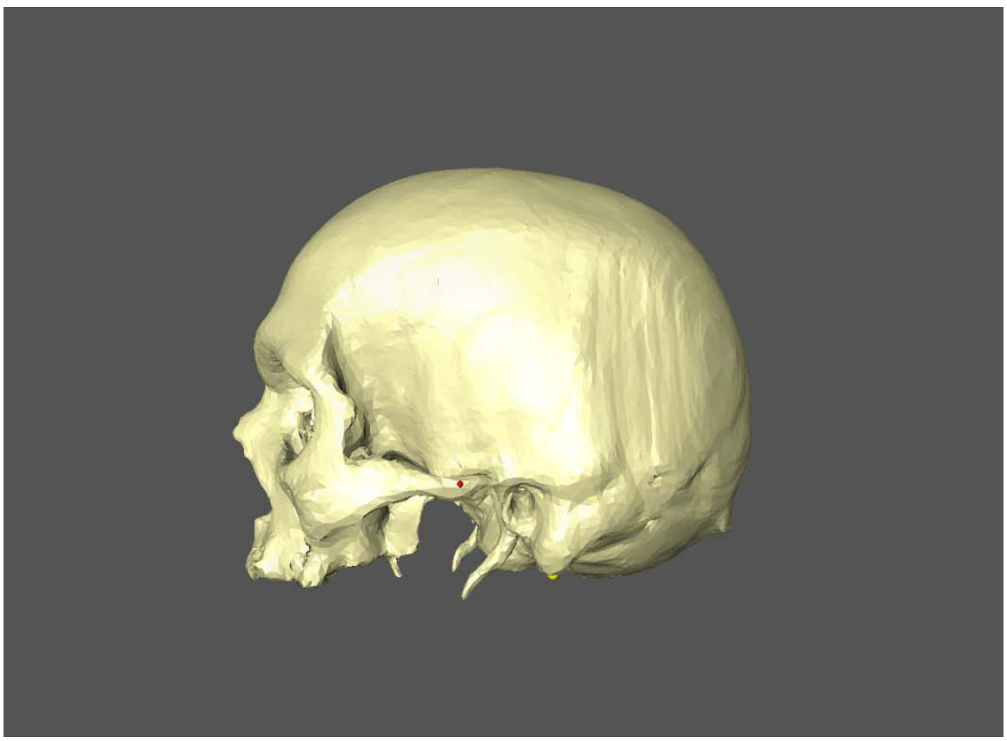

Figure 32 Right zygion and right mastoidale.

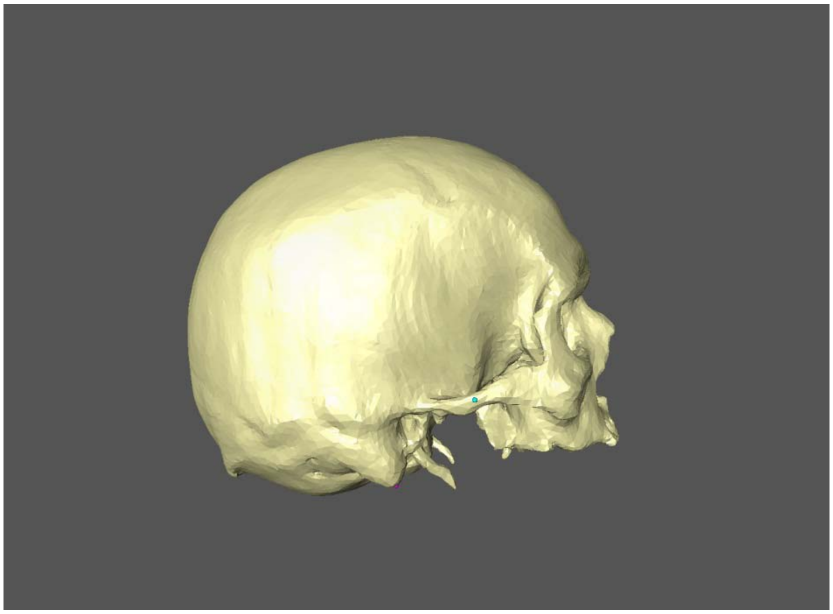

Figure 33 Calculated landmarks.

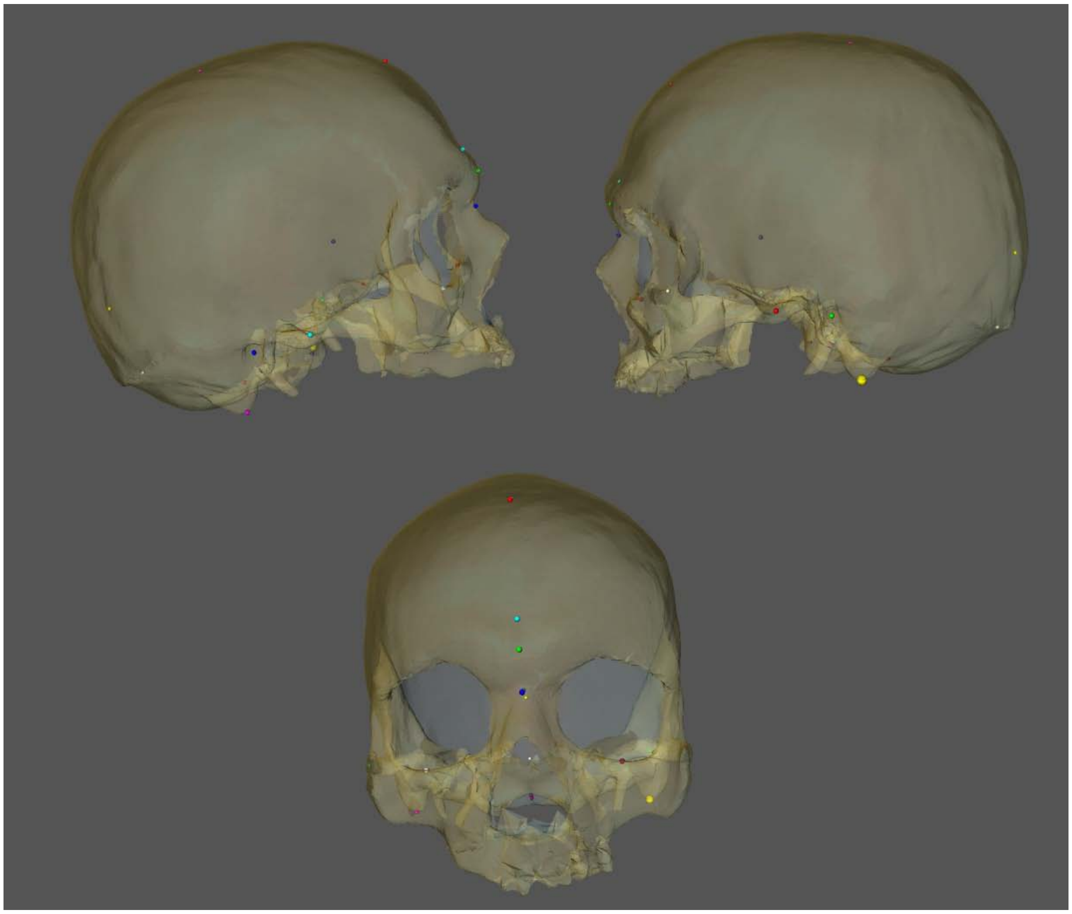

Figure 34 Vault thickness landmarks.

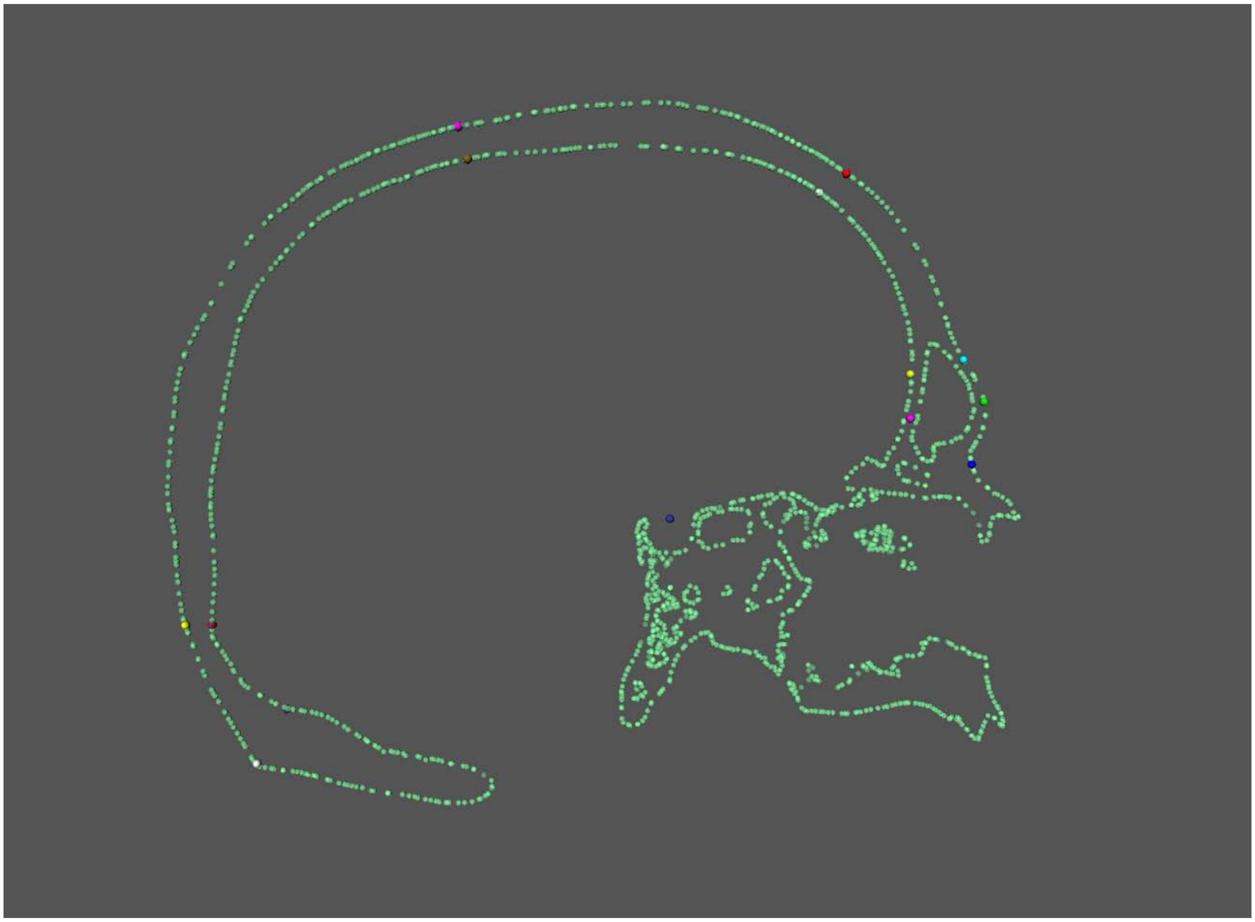

Figure 35 Vault Thickness landmarks.

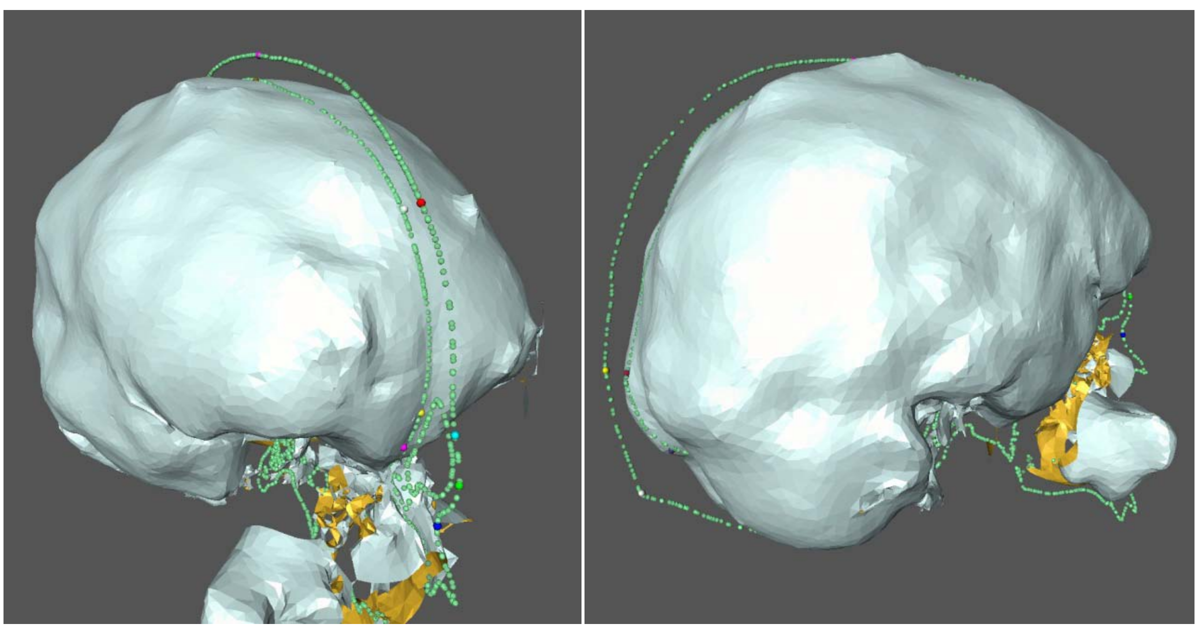

The following landmarks were located on the skull models:

1. *Basion*—most inferior posterior point in the midsagittal plane on the anterior rim of the foramen magnum.

2. *Gabella*—most anteriorly projecting point in the midsagittal plane at the lower margin of the frontal bone, which lies above the nasal root and between the superciliary arches.

3. *Inion*—most prominent point of the external occipital protuberance.

4. *Mastoidale*—lowest point of the mastoid process.

5. *Metopion*—point where the line that connects the highest points of the frontal eminences crosses the sagittal plane.

6. *Nasion*—the point of intersection of the naso-frontal suture and the midsagittal plane.

7. *Opisthioncranion*—most posteriorly protruding point of the occipital bone in the midsagittal plane.

8. *Opisthion*—the point at which the midsagittal plane intersects the posterior margin of the foramen magnum.

9. *Porion*—midpoint (centroid) of the external auditory meatus.

10. *Sella*—midpoint of the sella turcica.

11. *Supraglabella*—most posterior point in the midsagittal plane in the supraglabellar fossa; the concavity between glabella and metopion.

12. *Vertex*—the highest point on the cranial vault in the midsagittal plane (used in lieu of bregma on account of the absence of sutures in some of the models).

13. *Zygion*—the most laterally positioned point on the zygomatic arches.

The following measurements were taken from these landmarks:

<u>Linear measurements (mm):</u>

1. Cranial base length (basion-nasion; BNL).

2. Maximum cranial length (glabella-opisthocranion; GOL).

3. Foramen magnum length (basion-opisthion; FOL).

4. Bizygomatic breadth (zygion-zygion; ZYB).

5. Mastoid height (porion to mastoidale, left and right; MDH).

6. Mastoid width—maximum width of the mastoid in the anterior-posterior direction.

7. Orbital height—greatest height of the orbit taken from points on the superior and inferior orbital margins (left and right; OBH).

8. Cranial height (vertex-basion; VB).

9. Frontal cord (vertex-nasion; VN).

10. Sella-Nasion (SN).

11. Sella-Basion (SB).

12. Mastoidale-Sella (left and right; MaS)

13. Mastoidale-Basion (left and right; MaB)

14. Glabella-Nasion (GN)

15. Glabella-Supraglabella (GSg)

16. Nasion-Supraglabella (NSg)

17. Glabella-Supraglabella-Nasion line—orthogonal distance from glabella to a line connecting supraglabella and nasion (G-SgN).

18. Glabellar projection index (GPI) = (glabella to supraglabella-nasion)*100/ (supraglabella to nasion).

19. Glabella superior-inferior projection index—a measure of the location of glabella along the midsagittal plane; G-SI-PI = GSg/GN.

<u>Angular measurements (°):</u>

20. Angle between the lines connecting glabella-metopion and sella-nasion (GM-SN).

21. Angle between the lines connecting glabella-metopion and basion-nasion (GM-BN).

22. Angle between the lines connecting glabella-sella and glabella-metopion (GS-GM).

23. Angle between the lines connecting inion-opisthocranion and sella-nasion (IOp-SN).

24. Angle between the lines connecting inion-opisthion and inion-opisthocranion (IO-IOp).

25. Angle between the lines connecting glabella-sella and glabella-nasion (GS-GN).

26. Angle between the lines connecting glabella-sella and sella-nasion (GS-SN).

27. Angle between the lines connecting sella-nasion and sella-mastoidale (right and left; SN-SMa).

28. Angle between the lines connecting inion-opisthion and basion-nasion (IO-BN).

29. Angle between the lines connecting inion-opisthocranion and basion-nasion (IOp-BN).

30. Angle between the lines connecting glabella-nasion and glabella-supraglabella (GN-GSg).

31. Mastoid angle—angle between the lines connecting mastoidale and the most anterior and posterior points where the mastoid contacts the cranial base (left and right; LMA and RMA).

32. Angle between the lines connecting sella-nasion and sella-mastoidale (right and left; SN-SMa).

<u>Thickness measurements (mm):</u>

33. Vault thickness at glabella (VTG).

34. Vault thickness at supraglabella (VTSg).

35. Vault thickness at metopion (VTM).

36. Vault thickness at opisthocranion (VTOp).

37. Vault thickness at inion (VTI).

38. Vault thickness at vertex (VTV).

The measurements were calculated once on the atlas and then automated across all models in the atlas. Measurements were tested for discriminating capability using a measurement of separation. Stepwise multilinear regression was used to determine the best variables to include in the discriminant model ($p \leq 0.1$ was used as the threshold for variables to be added during the regression). The selected variables were fed to a discriminant analysis classifier, and the classification percentage for each sex and total classification rate were calculated using leave-one-out cross-validation.

F. Testing and Validation

In order to determine if the endocranial measurements obtained from the cranial atlas can be used in a lab without access to a CT scanner, subset of the Bass Collection crania (n=30) were used for a test study. Lateral x-rays were generated from the CT scans, and the radiographic measurements were taken with the freely available ImageJ software (http://rsbweb.nih.gov/ij/). In addition, the computer-automated ectocranial measurements were compared with measurements taken with calipers. Paired t-tests (α=.05) were used to test for significant differences between the two sets of measurements, and percent error was calculated to examine the magnitude of the differences.

$$\%\ \text{error} = \frac{\left|\text{caliper or radiograph measurement} - \text{bone atlas measurement}\right|}{\text{bone atlas measurement}} * 100\%$$

III. Results

A. Global Analysis

Table 1 presents the results of the Principal Components Analysis (PCA) of the unscaled data and on the data treated with the Generalized Procrustes Analysis. The results of the unstandardized PCA show that the first principal component (size) accounts for 35% of the variation in male crania and 41% in females. The first principal component is generally considered the percentage of variation attributed to differences in size. The first principal component (

Figure 36) shows that this variation is largely on account of differences in size of the glabellar region and cranial length, as well as mastoid size and facial breadth across the zygomatic bones (areas of high dimorphism are indicated by warm colors and areas of low dimorphism are shown with cool colors). Principal components 2-10 account for an additional 38% of the variance in males and 34% in females. The second and third principal components are primarily capturing differences in the occipital region and in the zygoma, particularly the right zygomatic (Figure 37, Figure 38). The fourth principal component is showing differences in cranial breadth and in the zygoma, particularly the left zygomatic (Figure 39). Twenty principal components explain roughly 85% of the total variance, and 40 principal components account for 95% (see Table 1). Examined together PC1-40 highlight the differences in the glabellar region, zygomatics, and in cranial length (Figure 40). When the first principal component is removed, the shape differences in the glabellar region and in the zygoma are primarily apparent (Figure 41).

The results from the atlases with the GPA-PCA treatment to remove the effects of scale are presented in Table 1 and Figure 42- 47. The first principal component picks up the differences in shape of the occipital region, they zygomatics (especially the right side) and cranial breadth (Figure 42). The second principal component is similar to the first (Figure 43), but PC3 begins to pick up differences in the left zygomatic (Figure 44), while PC4 highlights the occipital differences again and brings in the glabellar region (Figure 45). Examining PC1-40 shows the differences in the shape of the glabellar region, and, to a lesser degree, in the inclination of the mastoid (Figure 46). Several of the targeted features are consistent with areas scored in nonmetric sex assessment (occiput/nuchal region, glabella, and mastoid).

Table 1. PCA results for unscaled data and data scaled with the GPA treatment.

	Accumulated Variance (%) Non-Normalized		Accumulated Variance (%) Normalized	
PC	**Male**	**Female**	**Males**	**Females**
1	35	41	14	14
2	44	50	24	23
3	52	55	31	31
4	56	60	37	37
5	60	63	41	42
6	64	66	46	47
7	67	68	49	50
8	69	71	53	53
9	71	73	56	56
10	73	75	58	59
11	75	76	60	61
12	77	78	62	63
13	78	79	64	65
14	79	81	66	67
15	80	82	67	69
16	82	83	68	70
17	83	84	69	72
18	84	85	71	73
19	84	85	72	74
20	85	86	73	75
40	94	95	84	88

Figure 36. Unstandardized PCA results: PC1.

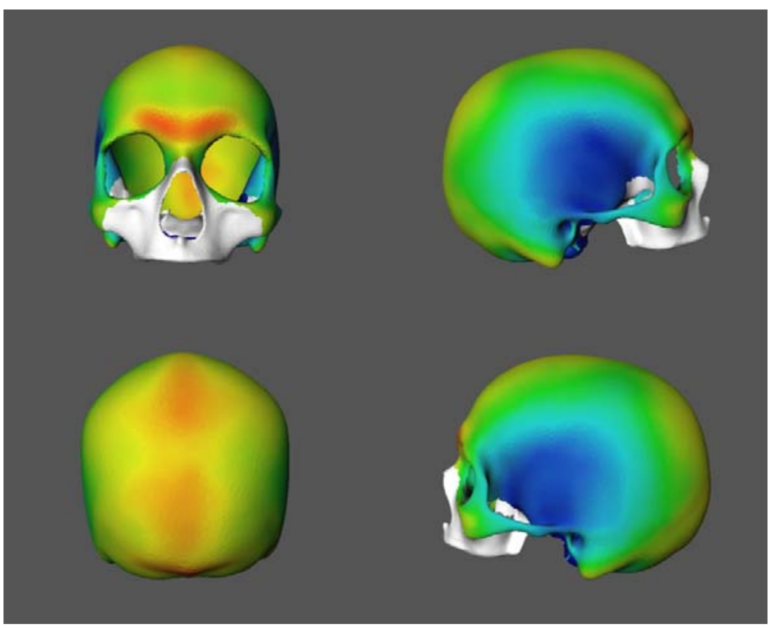

Figure 37. Unstandardized PCA results: PC2.

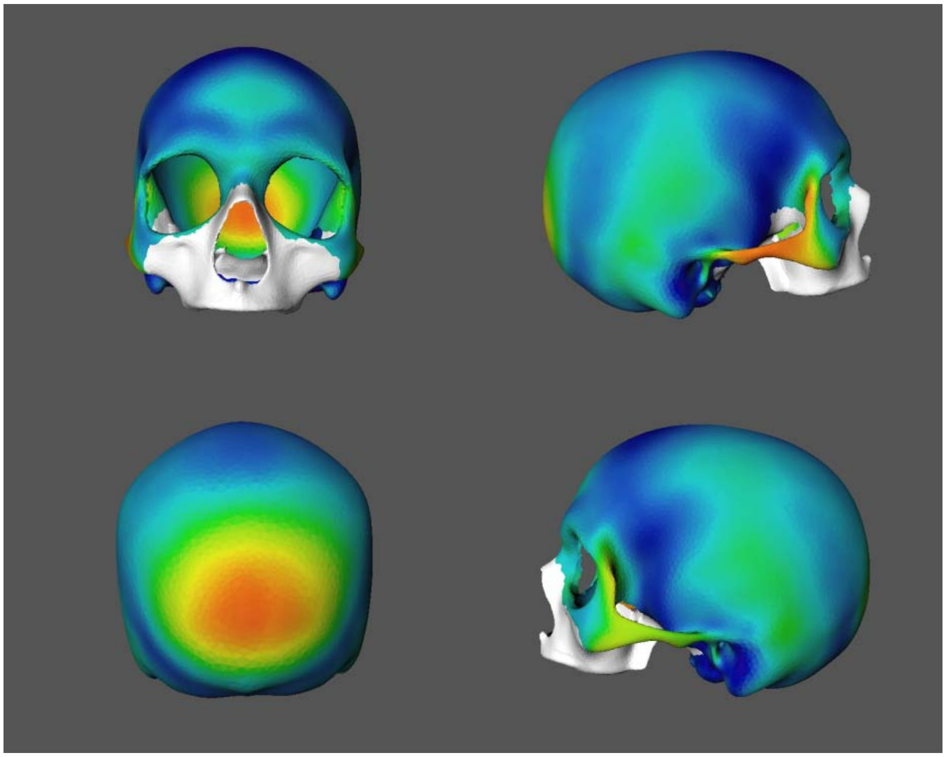

Figure 38. Unstandardized PCA results: PC3.

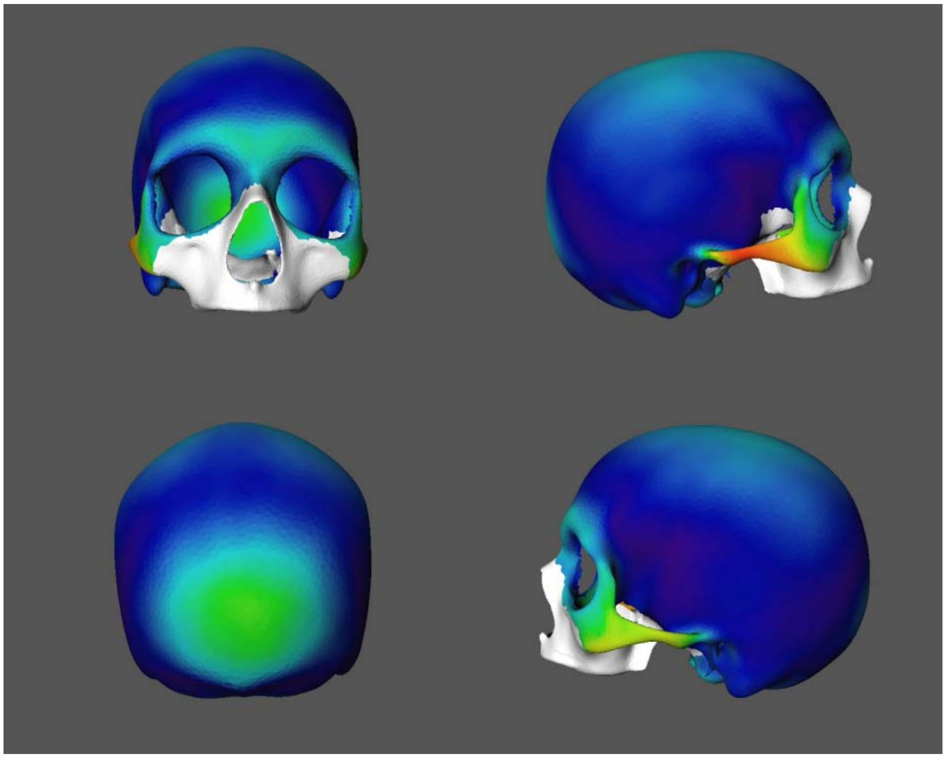

Figure 39. Unstandardized PCA results: PC4.

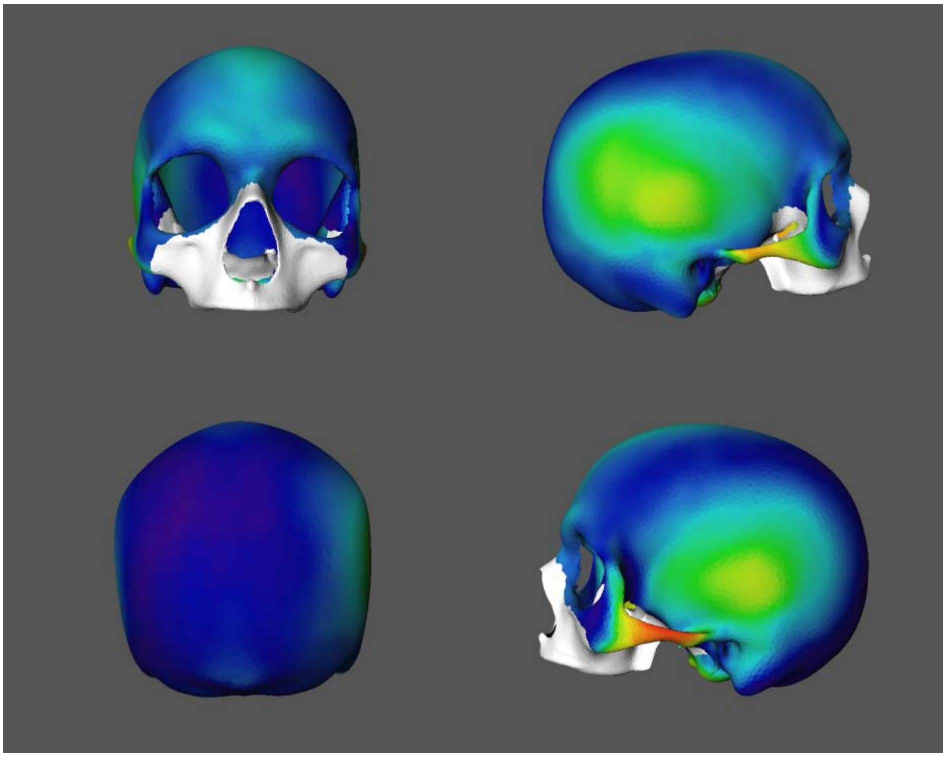

Figure 40. Unstandardized PCA results: PC1-40.

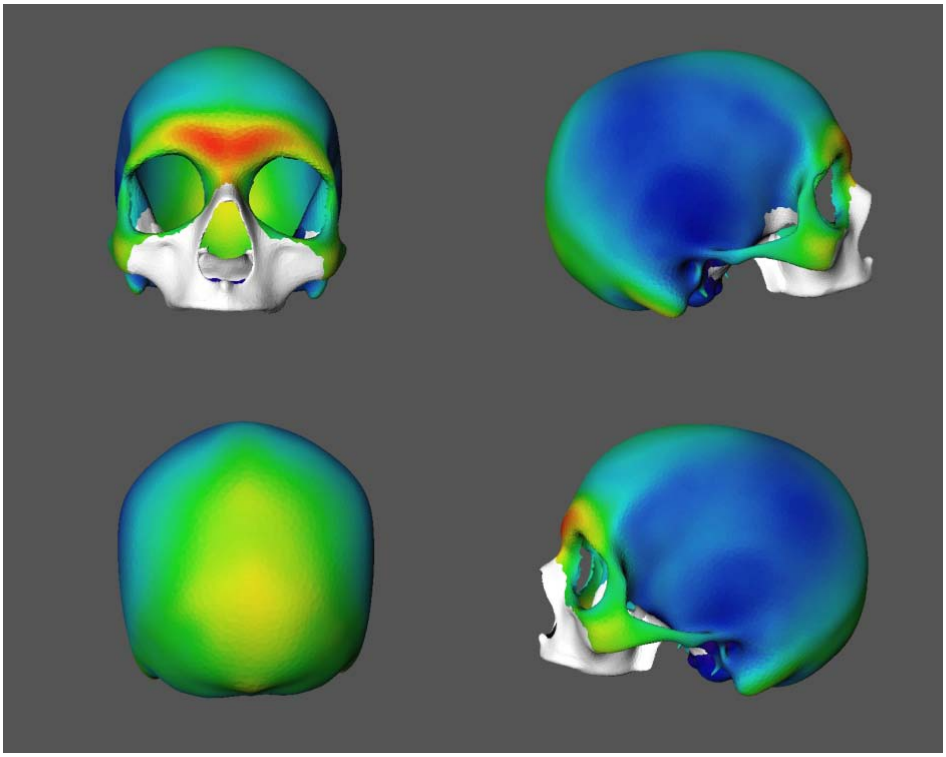

Figure 41. Unstandardized PCA results: PC2-40.

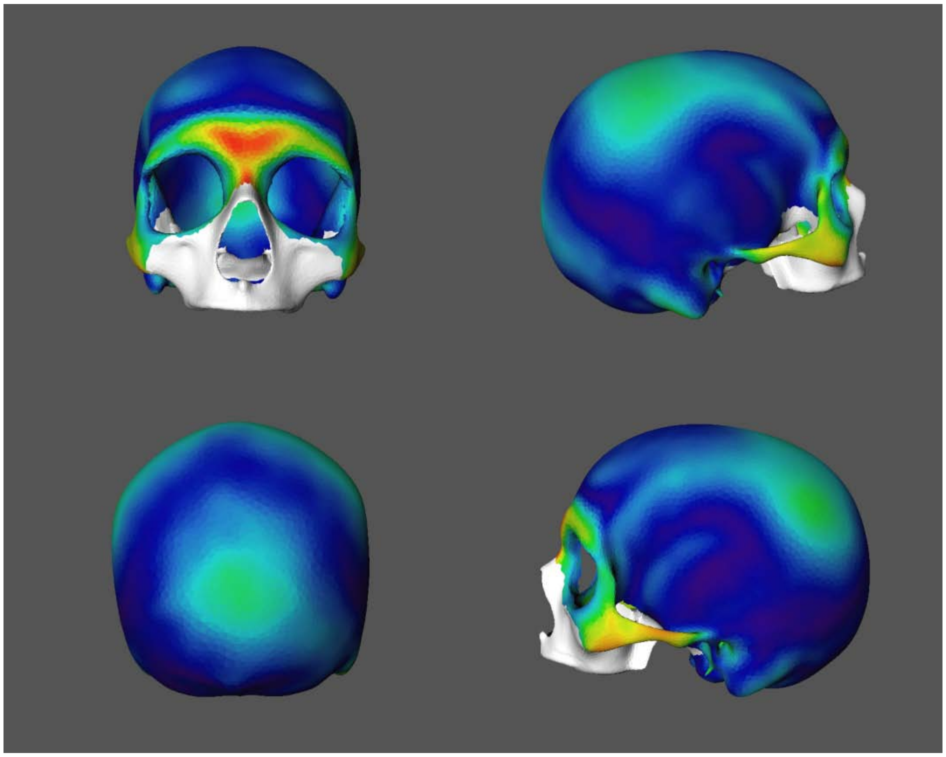

Figure 42. GPA-PCA results: PC1.

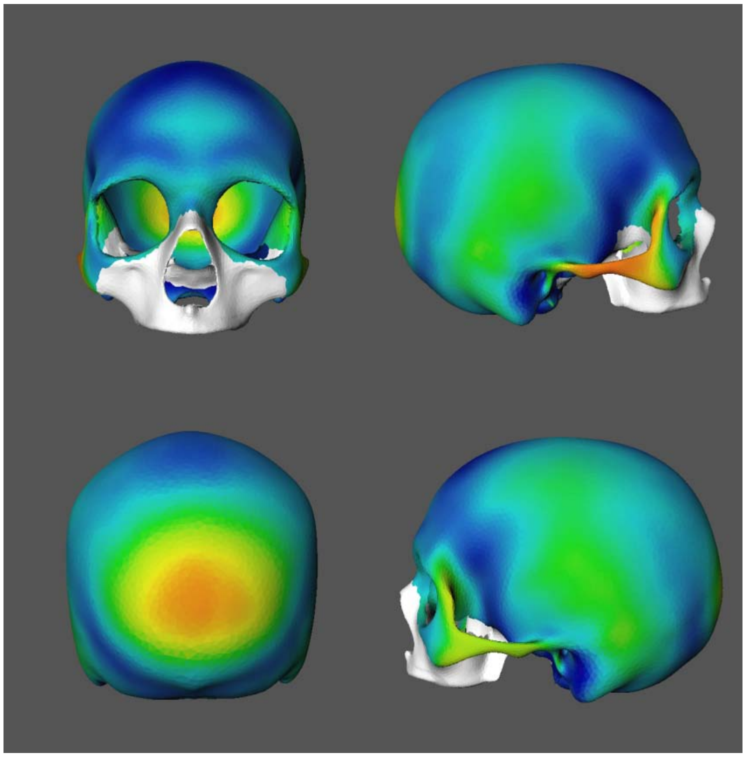

Figure 43. GPA-PCA results: PC2.

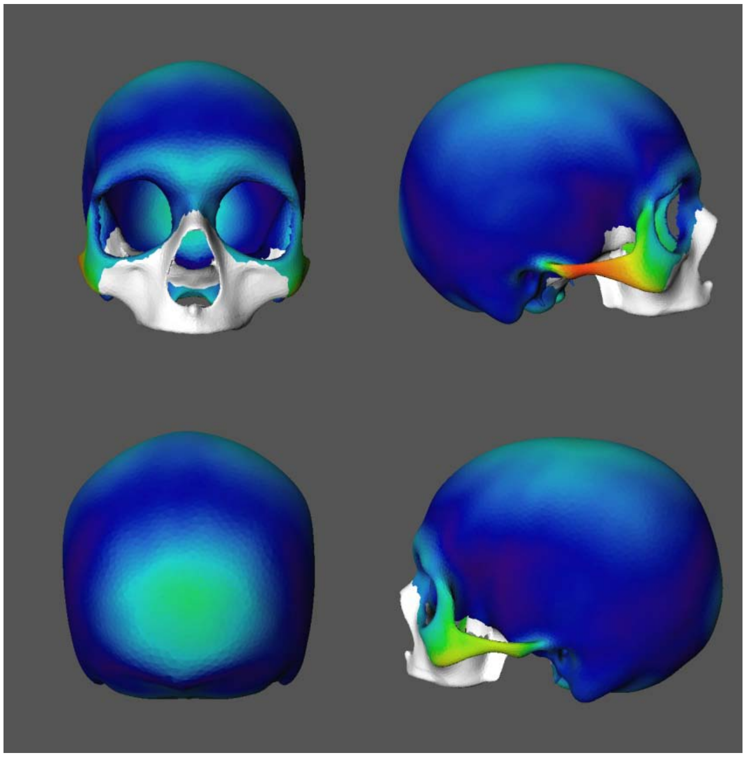

Figure 44. GPA-PCA results: PC3.

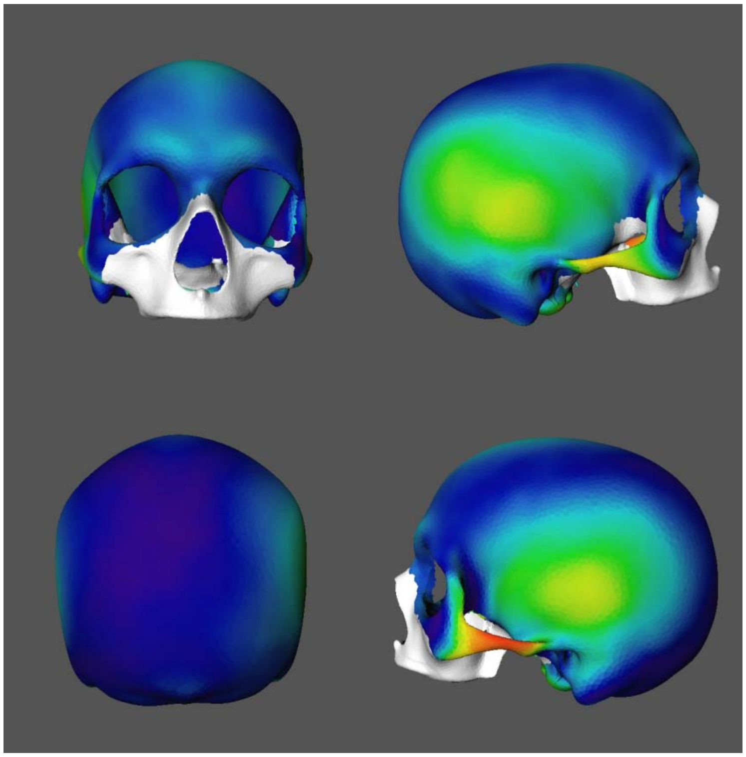

Figure 45. GPA-PCA results: PC4.

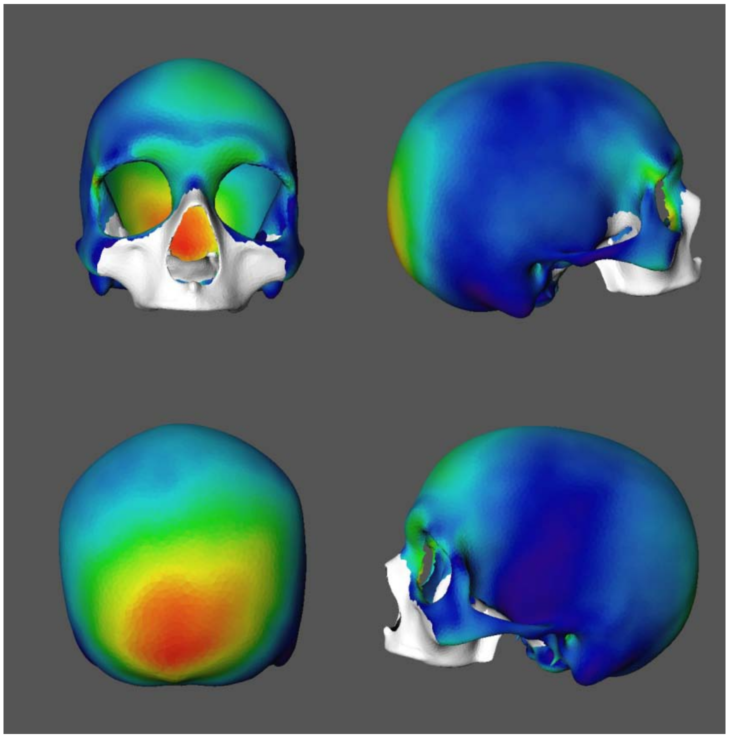

Figure 46. GA-PCA results: PC1-40.

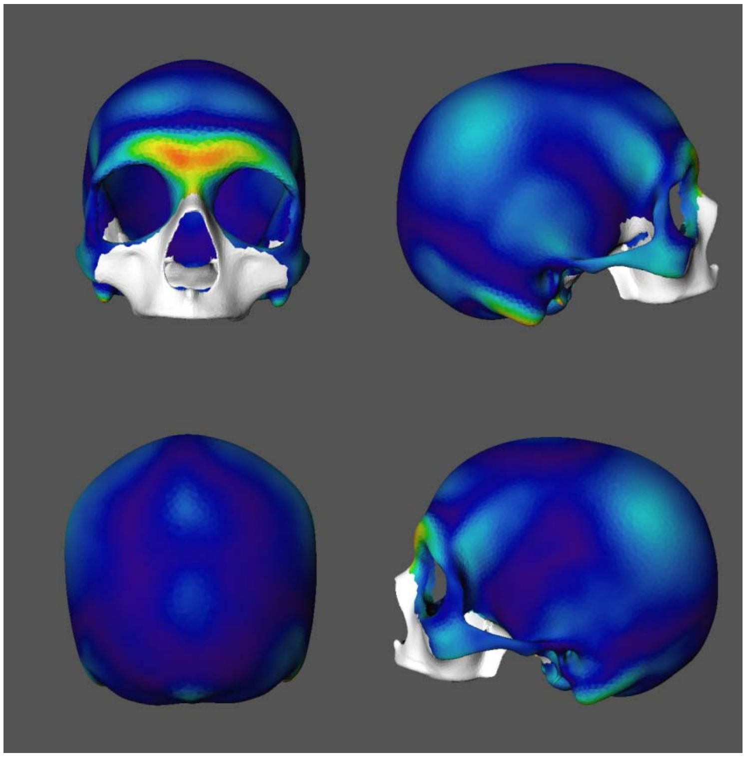

B. Local Analysis

The male and female means, standard deviations, and the separation index of each of the 42 variables are reported in Table 2. The separation index is a measure of the discriminating ability of each variable, defined as |Xm-Xf|/(sdm+sdf) (Maynard-Smith et al. 1961). The proportion correct classification is based on the cumulative normal curve, the area to the left of the separation index. The expected values normally agree well with empirical classification (compare to Table 3 for GPI, ZYB, and BNL). It should be noted that these are univariate statistics and do not necessarily predict which variables will enter a multivariate model, because the univariate statistics do not account for covariation.

The univariate statistics do show which areas of the skull are the most dimorphic and these areas agree with those found in the global analysis. The best variables (GPI and GN-GSg) are measures of glabellar projection, both of which can classify well above 80%. Face breadth has long been known to be a good discriminator, and ZYB alone can also discriminate above 80%. Beyond that we see that sagittal length measurements are important (GOL, BNL). Again, these areas were all highlighted in the various principal components of the global analysis. The vault thicknesses alone are only moderately effective, and the angles of the vault range from moderate to poor. The worst, the angle between the lines connecting inion-opisthocranion and sella-nasion (IOp-SN) shows no dimorphism at all, resulting in sexing accuracy no better than random.

Table 2. Descriptive statistics. Means and standard deviations of 42 variables for 140 males and 81 females, sorted by separation index. The separation index is a measure of discriminating ability of each variable. Proportion correct estimated from cumulative normal distribution. Refer to the listed measurements in Methods.

Variable	Male mean	Male SD	Female mean	Female SD	Separation index*	Proportion correct**
GPI	11.457	3.505	5.917	1.813	1.042	0.851
GN-GSg	27.827	7.052	16.144	4.925	0.975	0.835
ZYB	131.632	4.399	124.203	3.579	0.931	0.824
BNL	103.614	4.121	96.814	3.280	0.919	0.821
G-SgN	2.423	1.042	1.247	0.402	0.814	0.792
GOL	187.385	6.427	176.995	6.811	0.785	0.784
LM-S	54.173	2.453	50.642	2.924	0.657	0.744
RM-S	53.953	2.326	50.154	3.573	0.644	0.740
SN	66.740	4.829	60.933	4.485	0.623	0.733
GS-GM	79.825	3.903	84.944	4.351	0.620	0.732
GSg	8.365	3.038	6.396	0.224	0.604	0.727
G-SI-PI	0.669	0.283	0.444	0.106	0.578	0.718
VB	141.911	5.421	136.600	4.752	0.522	0.699
MDH-L	28.765	2.929	26.023	2.463	0.508	0.694
MDH-R	27.910	2.790	25.011	2.924	0.507	0.694
VTG	18.233	4.417	14.839	2.724	0.475	0.683
VTI	16.391	2.715	14.221	2.968	0.382	0.649
FOL	37.569	2.393	35.852	2.455	0.354	0.638
VTM	7.449	1.477	8.614	1.827	0.352	0.638
SB	50.428	4.980	47.467	4.654	0.307	0.621
OBH-R	39.746	2.678	37.852	3.563	0.304	0.619
SN-SM-L	118.794	3.272	120.914	3.726	0.303	0.619
IO-IOp	128.046	6.654	131.820	5.875	0.301	0.618
GN	13.184	3.065	15.237	3.817	0.298	0.617
GM-SN	110.212	4.009	107.948	3.938	0.285	0.612
VN	139.079	8.025	135.191	6.634	0.265	0.605
IO-BN	129.116	6.793	125.864	6.114	0.252	0.599
SN-SM-R	119.139	3.225	120.940	4.304	0.239	0.595
GM-BN	93.604	3.922	95.313	3.646	0.226	0.589
GS-GN	61.414	5.230	63.781	5.320	0.224	0.589
MW-L	35.596	2.424	34.544	2.423	0.217	0.586
SN-SB	123.879	5.527	126.234	5.541	0.213	0.584
OBH-L	37.870	3.379	36.683	2.787	0.193	0.576
MW-R	37.436	2.293	36.702	2.394	0.157	0.562
VTOp	9.242	2.378	8.948	1.871	0.069	0.528
NSg	20.902	4.098	21.440	3.885	0.067	0.527
VTSg	13.413	2.733	13.067	2.944	0.061	0.524
IOp-BN	102.838	4.979	102.316	4.867	0.053	0.521
VTV	7.426	1.410	7.537	1.206	0.043	0.517
IOp-SN	100.978	5.298	100.945	5.709	0.003	0.501

* Separation index= |Male mean-Female|/(male SD + female SD)
** Estimate of correct classification assuming normal distribution

Table 3 shows several discriminant models. The best model gets 97.3% accuracy with 11 variables (note: SN-SML cannot be measured on a radiograph). The next best model achieves 95.5% overall classification accuracy with just 8 variables, all of which are related to size differences. A model utilizing just shape variables (two angles and glabella projection index) classifies 86.5% of the cross-validated sample accurately; a model with variables capturing the shape of the brow ridge (GN-GSg and G-SgN) classifies 83.8% accurately. The glabella projection index alone gets 82%, as does basion-nasion length (cranial base length) and bizygomatic breadth (83%). With the exception of SN-SML, all of these measurements are taken easily with calipers and/or on a lateral or anterior-posterior radiograph. What is interesting is that vault thickness at metopion (VTM) enters in the two best models, despite having a relatively low univariate separation index. That is presumably because its sex dimorphism is opposite that of other direct measurements, females have larger values; VTM classifies alone at 69%. Table 4 gives the coefficients for the discriminant functions.

Table 3. Cross-validated LDA results. Best linear discriminant models using stepwise variable selection.

Model Variables	Combined	Male	Female
BN, ZYB, LMH, IO-IOp, SN-SML, VTM, GOL, VN, GSg, GPI, LMS	97.3	96.5	98.8
BN, ZYB, LMH, VTM,GOL, VN, GSg, LMS	95.5	95.0	96.3
IO-IOp, SN-SML, GPI	86.5	87.9	96.3
GN-GSg, G-SgN	83.8	87.9	76.5
GPI	82.4	84.4	79.0
ZYB	82.9	89.4	71.6
BNL	82.0	86.5	74.1

Table 4 Discriminant function coefficients and constants.

Variable	Coefficient	Variable	Coefficient	Variable	Coefficient	Variable	Coefficient
BN	0.4363	BN	0.3320	IO-IOp	-0.0967	GN-GSg	0.3765
ZYB	0.2364	ZYB	0.2723	SN-SML	-0.1946	G-SgN	-0.7724
LMH	0.3213	LMH	0.2550	GPI	0.6172		
IO-IOp	-0.1306	VTM	-1.1147				
SN-SML	-0.2293	GOL	0.2142				
VTM	-1.1781	VN	-0.1119				
GOL	0.1662	GSg	0.1941				
VN	-0.0858	LMS	0.3487				
GSg	-0.4637						
GPI	0.8194						
LMS	0.3341						
Constant	-67.6769	Constant	-108.7266	Constant	31.0806	Constant	-6.2977

C. Validation

As this study is an investigation of primarily non-traditional craniometrics (i.e. angles, endocranial measurements, and vault thickness), a limited number of overlapping measurements were available for comparing caliper measurements and virtual measurements: BNL, ZYB, FOL, GOL. MDH and OBH were not compared, as these measurements were calculated differently on the atlas. The paired t-test results are presented in Table 5. The Pearson correlation coefficients between the atlas and caliper measurements is high, but all measurements registered significantly different except FOL (foramen magnum length). Presumably this is because the hypothesized difference between the measurements is 0, thus making the paired t-test a highly sensitive measure of difference. Table 6 summarizes the percent error calculations of the measurements. The mean, median, and modal percent error is less than 2% in the majority of the measurements (the modal value is 0%). Note that the highest value obtained was for FOL (14.29%, n=1). All other values are <6%. Interestingly, FOL was the only measurement that did not register significantly different in the paired t-test; however, it has the Pearson's r (0.89). Considering the sensitivity of the paired t-test as it was measured (hypothesized mean difference = 0), which does not allow for observer error, compared to the percent error calculations, we conclude that there is general agreement between manual and virtual measurements and between the virtual models and true cranial form.

A subset of the endocranial and angular measurements captured in the most accurate discriminant functions were taken from lateral radiographs. The results of the percent error calculations are shown in Table 77. The measurements with the highest percent error are those containing sella, thereby suggesting the need for a more standardized method of locating this landmark on a radiograph. While some landmarks are easy to locate on radiographs (glabella, supraglabella, nasion), others are more difficult (sella, basion), and locating them accurately depends largely on the quality of the radiograph. Future research will work on refining the radiograph measurement definitions and protocols.

Table 5. Paired t-test results: caliper versus atlas measurements.

	ZYB		**GOL**		**FOL**		**BNL**	
	Caliper	*Atlas*	*Caliper*	*Atlas*	*Caliper*	*Atlas*	*Caliper*	*Atlas*
Mean	128.10	129.81	182.99	184.20	36.620	36.73	101.973	101.41
Variance	37.12	34.84	76.70	75.36	6.828	6.60	28.058	26.80
Observations	187	187	187	187	187	187	187	187
Pearson Correlation	0.977		0.987		0.891		0.958	
Hypothesized Mean Difference	0		0		0		0	
DF	186		186		186		186	
t Stat	-18.067		-11.941		-1.205		5.050	
P(T<=t) one-tail	4.280E-43		4.567E-25		0.115		5.252E-07	
t Critical one-tail	1.653		1.653		1.653		1.653	
P(T<=t) two-tail	8.559E-43		9.134E-25		0.230		1.050E-06	
t Critical two-tail	1.973		1.973		1.973		1.973	

Table 6. Percent error between atlas and caliper measurements (absolute values).

	ZYB	GOL	FOL	BNL
Mean % error	1.39	0.75	1.83	1.20
Median % error	1.48	0.56	2.56	0.99
Mode % error	0.00	0.00	0.00	0.00
Standard Deviation	0.81	0.66	1.98	1.04
Low % value	0.00	0.00	0.00	0.00
High % value	4.27	3.61	14.29	6.67

Table 7. Percent error between atlas and radiograph measurements (absolute values).

	SN	GS-GN	GM-SN	GM-BN	VTM
Mean % error	4.020	8.637	3.772	0.750	0.407
Median % error	3.030	9.722	3.704	1.111	0.000
Mode % error	0.000	9.722	3.704	0.000	0.000
Standard Deviation	5.029	5.741	2.734	2.707	13.159
Low % value	0.000	1.449	0.000	0.000	0.000
High % value	16.949	25.758	10.714	7.447	28.571

IV. Conclusions

A. Discussion of Findings

This study has confirmed that, with respect to cranial sex dimorphism, size contributes a significant portion of the variation (35-41% according to the unscaled PCA). However, shape is more important than was once thought. Important size-related variables that were captured in the highest-yielding discriminant functions were bizygomatic breadth (ZYB), cranial base length (BNL), and maximum cranial length (GOL). In addition, vault thickness is a sexually dimorphic feature, with females having a thicker vault than males in the frontal region and vice versa in the occipital region. This was also documented by Ishida and Dodo (1990) and by Ross et al. (1998), who also found that female vault thickness increases with age, and male vault thickness decreases with age. Ross et al. (1998) attributed the increase in female vault thickness to hyperostosis frontalis interna (HFI), a condition of unknown pathogenesis with a female to male ratio of 100:1. Furthermore, they concluded that vault thickness in the parietal and frontal regions is not sexually dimorphic until the onset of HFI (usually around the age of 50). The average age of the females in the present study was 66.4 years and the males were 64.1 years. HFI should not directly affect our frontal thickness measurements, since they were taken in the midline where the superior sagittal sinus suppresses its development. However, the significant sex dimorphism in vault thickness of the frontal region could be an indirect consequence of HFI.

Our results generally echo previous studies and support our predictions in that bizygomatic breadth, dimensions of the glabellar region, and the occiput are highly sexually dimorphic areas. While frontal bone morphology and bizygomatic breadth appear to typify sex dimorphism across populations (i.e. these variables are more universally dimorphic) (Franklin et al. 2004), there are population-specific aspects of sex dimorphism, as well. For example, a single variable (IOp-BN angle) classified 94% of Taiwanese adults correctly (Hsiao et al. 1996) and was similarly dimorphic in children and adolescents (Hsiao et al. 2010). However, this variable was not selected in a French sample (Veyre-Goulet et al. 2008) and only classified 56% of the present sample correctly and was not included in any of the best discriminant models.

The best attainable classification rates from discriminant functions in the Fordisc program using traditional measurements vary from just under 90% to a maximum of 91.8% using all variables. This study was able to attain 97.3% accuracy with an 11-variable model and 95.5% overall classification accuracy with just 8 variables, all of which are related to size differences. A model utilizing just shape variables (two angles and glabella projection index) classifies 86.5% of the cross-validated sample accurately; a model with variables capturing the shape of the brow ridge (GN-GSg and G-SgN) classifies 83.8% accurately. The glabella projection index alone gets 82%, as does basion-nasion length (cranial base length) and bizygomatic breadth (83%). in this study are higher than reported to date in the literature for the American population. Interestingly, the left side is consistently selected as a better classifier in the case of bilateral measurements, thus indicating the possibility of asymmetry in sexual dimorphism.

The cranial atlas is a powerful statistical tool that permits a thorough morphometric analysis across 20,000 homologous points, automated feature finding and landmarking, and computer automated measurement extraction. Statistical atlases are ideal for analyzing large datasets, conducting shape analyses, and for conducting exploratory analyses that assist in developing and fine-tuning more specific methods. This study of cranial sexual dimorphism has demonstrated how bone atlases can be used to detect areas of significant variation between populations, calculate measurements rapidly across large datasets, and improve classification rates over traditional methods. We intend to continue to use the cranial atlas to explore further questions about sexual dimorphism, including the degree to which sex dimorphism is asymmetric in the American population. Furthermore, we are presently exploring its capabilities as a tool for fragment reconstruction.

B. Implications for Policy and Practice

One of the main components of the biological profile that forensic anthropologists develop from unidentified human skeletal remains is sex. It is well known, in the current state of the art, that postcranial elements are generally superior to cranial elements for sex estimation. Therefore, when cranial and postcranial elements are both present, forensic anthropologists typically give more weight to postcranial elements, especially os coxae. However, skeletal forensic cases often consist of a skull only, or a skull and fragmentary or incomplete postcranial remains. There do not appear to be concrete data concerning how frequently sex must be estimated solely from the cranium, either because it is the only element represented, or because the postcranial remains are too fragmentary to be useful. However, it is our experience at the University of Tennessee that crania are over represented in forensic casework. We have attempted to provide a more solid basis for this impression by querying the Forensic Anthropology Data Bank, which contains information submitted by forensic anthropologists around the country. The results are shown in Table 7.

Table 8. Co-occurrence of skull with various sexable postcranial elements in the Forensic Anthropology Data Bank (N= 848-857).

Element Combination	N	%
Skull with ilium or pubis	181	21.3
Skull without ilium or pubis	471	55.5
Skull with femur	202	23.6
Skull without femur	405	47.3
Skull with humerus	188	22.1
Skull without humerus	391	45.9
Skull with no sexable postcranial elements	390	45.5

It is apparent that skulls accompanied by specific postcranial elements are only about one-half as common as skulls without those elements. About 45% of skulls are unaccompanied by any sexable postcranial remains (i.e. a major long bone or os coxae). There is potential bias in these results in that skulls may be submitted to us for analysis without including postcranial remains, even though they may be present. There are, however, some reasons to accept the idea that crania are over represented in forensic casework:

- Crania are easily recognized as human by untrained observers, while postcranial elements are not as readily recognizable.
- Crania are less susceptible to carnivore damage than postcranial remains.

As outlined in the literature review, the success rate for sexing crania using traditional methods is 90% or less. Since the need to sex skeletal remains from the skull alone is a common occurrence, forensic anthropologists should have sexing criteria that are as reliable as possible. This study has provided a validated methodology for forensic anthropologists to estimate sex in modern Americans. Lateral radiographs are generally available to forensic anthropologists and, as shown here, introduce a deeper understanding of cranial sexual dimorphism into forensic practice without the need for expensive equipment or computer programs.

Finally, the American population is known to be changing rapidly, both demographically and morphologically. The William M. Bass Donated Collection is the largest and most well-documented collection of modern skeletons in the United States. It is no longer possible to rely on nineteenth century collections such as Terry and Hamann-Todd for forensic criteria. This study provides sexing criteria for modern Americans of European ancestry. More broadly, it has made the 3-D models of the crania available for access by anyone, thereby establishing the beginning of an online, virtual collection for cranial morphology that will have utility well beyond what is set forth in this project.

C. Implications for Further Research

This study was limited to Whites. It is obviously important to investigate other ancestries as well as other American and European populations. There is preliminary evidence from Fordisc that Whites are more dimorphic than Blacks who are more dimorphic than Hispanics. The general nature of variation in sex dimorphism variation should be investigated so there is a better understanding of where the greatest dimorphism is located in different populations.

V. References Cited

Agathos A, Pratikakis I, Perantonis S, Sapidis NS. 2010. Protrusion-oriented 3D mesh segmentation. Visual Computer 26(1):63-81.

Arun K, Huang T. 1987. Least-Squares Fitting of Two 3D Point Sets, IEEE PAMI. 9(5):698-700.

Ayers HG, Jantz RL, Moore-Jansen PH. 1990. Giles and Elliot race discriminant functions revisited: A test using recent forensic cases. In: Gill GW, Rhine S, editors. Skeletal Attribution of Race. Albuquerque, NM: Maxwell Museum of Anthropology, Anthropological Papers No. 4. p 65-71.

Bigoni L, Veleminska J, and Bruzek J. 2010. Three-dimensional geometric morphometric analysis of cranio-facial sexual dimorphism in a Central European sample of known sex. Homo-Journal of Comparative Human Biology 61(1):16-32.

Bishop CM. 2006. *Pattern Recognition and Machine Learning*. New York: Springer.

Dayal M, Bidmos M. 2005. Discriminating sex in South African blacks using patella dimensions, J Forensic Sci 50(6): 1294-97.

Dayal M, Spocter MA, Bidmos MA. 2008. An assessment of sex using the skull of Black South Africans by discriminant analysis. Homo 59:209-21.

France DL. 1998. Observational and metric analysis of sex in the skeleton. In: Reichs KJ, editors. Forensic Osteology. Springfield, IL: Charles C. Thomas. p 163-86.

Franklin D, Milne N, Freedman L. 2004. A geometric morphometric study of cranial sexual dimorphism in selected indigenous populations of South Africa. Am J Phys Anthrop 123(38 Suppl): 96.

Franklin D, Freedman L, Milne N. 2005. Three-dimensional technology for linear morphological studies: a re-examination of cranial variation in four southern African indigenous populations. Homo 56:17-34.

Franklin D, Freedman L, Milne N, and Oxnard CE. 2006. A geometric morphometric study of sexual dimorphism in the crania of indigenous southern Africans. South African Journal of Science 102(5-6):229-238.

Gapert R, Black S, Last J. 2009a. Sex Determination from the Occipital Condyle: Discriminant Function Analysis in an Eighteenth and Nineteenth Century British Sample. Am J Phys Anthropol 138:384-394.

Gapert R, Black S, Last J. 2009b. Sex determination from the foramen magnum: discriminant function analysis in an eighteenth and nineteenth century British sample. Int J Leg Med 123:25-33.

Garvin HM, and Ruff CB. 2012. Sexual dimorphism in skeletal browridge and chin morphologies determined using a new quantitative method. American Journal of Physical Anthropology 147(4):661-670.

Giles E, Elliot O. 1963. Sex determination by discriminant function analysis of crania. Am J Phys Anthropol 21:53-68.

Graw M, Czarnetzki A, Haffner HT. 1999. The form of the supraorbital margin as a criterion in identification of sex from the skull: investigation based on modern skulls. Am J Phys Anthropol 108:91–96.

Hsiao TH, Chang HP, Liu KM. 1996. Sex determination by discriminant function analysis of lateral radiographic cephalometry. J For Sci 41:792-95.

Hsiao TH, Tsai SM, Chou ST, Pan JY, Tseng YC, Chang HP, Chen HS. 2010. Sex determination using discriminant function analysis in children and adolescents: a lateral cephalometric study. Int J Legal Med 124:155-60.

Ishida H, Dodo Y. 1990. Cranial thickness of modern and Neolithic populations in Japan. Hum Biol 1990 62(3):389-401.

Jantz RL, Meadows Jantz L. 2000. Secular change in craniofacial morphology. Am J Hum Biol 12:327-38.

Jantz RL. 2001. Cranial change in Americans. J Forensic Sci 46(4): 784-787.

Jantz RL, Wescott D. 2002. Assessing craniofacial secular change in American whites and blacks using geometric morphometry. Am J Phys Anthropol Suppl 34: 90-90.

Kemkes-Grottenthaler A. 2005. Sex determination by discriminant analysis: reliability of patella measurements, J Forensic Sci 147:129-33.

Komar DA, Buikstra JE. 2008. Forensic Anthropology: Contemporary Theory and Practice. New York, Oxford: Oxford University Press.

Konigsberg LW, Hens SM. 1998. Use of ordinal categorical in skeletal assessment of sex from the cranium. Am J Phys Anthropol 107:97-112.

Kranioti EF, Iscan MY, Michalodimitrakis M. 2008. Craniometric analysis of modern Cretan population. For Sci Int 180:110E1-110E5.

Krogman WM. 1962. The Human Skeleton in Forensic Medicine. Springfield IL: Charles C. Thomas.

Lestrel PE, Kanazawa E, and Wolfe CA. 2011. Sexual dimorphism using elliptical Fourier analysis: shape differences in the craniofacial complex. Anthropological Science 119(3):213-229.

Mahfouz M, Badawi A, Merkl B, Fatah EA, Pritchard E, Kessler K, Moore M, Jantz R. 2007a. 3D Statistical Shape Models of Patella for Sex Classification", Forensic Sci Int 173(2-3): 161-70.

Mahfouz M, Merkl B, Abdel Fatah EE, Booth R Jr., Argenson JN. 2007b Automatic methods for characterization of sexual dimorphism of adult femora: distal femur. Computer Methods in Biomechanics and Biomedical Engineering 10:447- 56.

Maynard-Smith S, Penrose LS, and Smith CAB. 1961. Mathematical Tables for Research Workers in Human Genetics. London: Churchill.

Moore-Jansen P, Ousley SD, and Jantz R. 1994. Data collection procedures for forensic skeletal material. Knoxville: The University of Tennessee Department of Anthropology and Forensic Anthropology Center.

Ramsthaler F, Kreutz K, and Verhoff MA. 2007. Accuracy of metric sex analysis of skeletal remains using Fordisc based on a recent skull collection. Int J Legal Med 121(6):477-482.

Ramsthaler F, Kettner M, Gehl A, and Verhoff MA. 2010. Digital forensic osteology: Morphological sexing of skeletal remains using volume-rendered cranial CT scans. Forensic Science International 195(1-3):148-152.

Rogers TL. 2005. Determining the sex of human remains through cranial morphology. J For Sci 50:493-500.

Rosas A, Bastir M. 2002. Thin-plate spline analysis of allometry and sexual dimorphism in the human craniofacial complex. Am J Phys Anthropol 117:236-45.

Ross AH, Jantz RL, and McCormick WF. 1998. Cranial thickness in American females and males. J Forensic Sci 43(2):267-72.

Saini V, Srivastava R, Rai RK, Shamal SN, Singh TB, and Tripathi SK. 2012. Sex Estimation from the Mastoid Process Among North Indians. Journal of Forensic Sciences 57(2):434-439.

Shamir A. 2008. A survey on mesh segmentation techniques. Computer Graphics Forum 27:1539-56.

Spradley MK, and Jantz RL. 2011. Sex Estimation in Forensic Anthropology: Skull Versus Postcranial Elements. Journal of Forensic Sciences 56:289-296.

Stewart TD. 1979. Essentials of Forensic Anthropology. Springfield IL: Charles C. Thomas.

Steyn M and Iscan M. 1998. Sexual dimorphism in the crania and mandibles of South African whites. Forensic Sci Int 98: 9–16.

Taubin G. 1995. Estimating the tensor of curvature of a surface from polyhedral approximation. Proceedings of the Fifth International Conference on Computer Vision.

Uytterschaut HT. 1986. Sexual dimorphism in human skulls. A comparison of sexual dimorphism in different populations. Hum Evol 1:243–50.

Veyre-Goulet SA, Mercier C, Robin O, Guerin C. 2008. Recent human sexual dimorphism study using cepahalometric plots on lateral teleradiography and discriminant function analysis. J For Sci 53:786-789.

Walker PL. 2008. Sexing skulls using discriminant function analysis of visually assessed traits. Am J Phys Anthropol 136:39-59.

Williams BA, Rogers TA. 2006. Evaluating the accuracy and precision of cranial morphological traits for sex determination. J For Sci 51:729-35.

VI. Dissemination of Research Findings

Completed:

Podium Presentation

American Academy of Forensic Sciences 63rd Annual Meeting, Chicago, IL, Feb. 21-26, 2011. *Shirley NR, Fatah EE, Jantz RL, Mahfouz MR*. 2011. **Improving Sex Estimation from the Cranium Using 3-Dimensional Modeling from CT Scans.** Proceedings of the American Academy of Forensic Sciences 17:355-56.

Manuscript Submission to Journal of Forensic Sciences (in review):

Improving Sex Estimation from Crania Using a Novel Three-dimensional Quantitative Method Emam ElHak Abdel Fatah, B.s.c., Natalie R. Shirley, Ph.D., Richard L. Jantz, Ph.D., Mohamed R. Mahfouz, Ph.D.

In Process:

Abstract Submissions

AAPA and AAFS—2013 Annual Meetings

Data Archiving

Uploading 3D cranial models—file link to be included on University of Tennessee Forensic Anthropology Center website and Biomedical Engineering server

Custom Data Sets for Fordisc 3.0

Variable sets that are especially effective at discriminating sex, and which are relatively easy for practitioners to obtain will be converted to custom data sets that can be imported into Fordisc. The custom data sets will be put on the Forensic Anthropology Center web and the Fordisc web site at Mercyhurst. These can then be downloaded, imported into Fordisc and used to classify sex. The user community will be alerted to the existence of these custom data bases by means of the Fordisc user email list.